CORRELATION OF COLOR AND ELECTRON SPIN RESONANCE IN DIAMOND

By

SAM E. GIUOCO

Bachelor of Science

Pan American College

Edinburg, Texas

1968

Submitted to the Faculty of the
Graduate College of the
Oklahoma State University
in partial fulfillment of
the requirements for
the Degree of
MASTER OF SCIENCE
May, 1969

CORRELATION OF COLOR AND ELECTRON

SPIN RESONANCE IN DIAMOND

Thesis Approved:

William J. Leivo
Thesis Adviser

N. V. V. J. Swamy

A. D. Durham
Dean of the Graduate College

ACKNOWLEDGMENTS

The author would like to express his sincere gradtitude to Dr. W. J. Leivo for his help, guidence, and constant encouragment during the course of this investigation. Special thanks are extended to Paul Klingsporn and William C. Steckelberg for their many enlightening discussions and suggestions regarding ESR in diamonds.

The semiconducting diamonds discussed in this study were kindly made available by Dr. J. F. H. Custers, Research Consultant, Industrial Distributers (1946) Limited. The author would like to express his appreciation to Dr. Custers for his continued interest and assistance in the diamond research at Oklahoma State University.

The support of the Research Foundation and the National Science Foundation is gratefully acknowledged.

Finally, the author would like to express his sincere appreciation to his wife, Barbara, whose understanding, patience, and tireless typing made this thesis possible.

TABLE OF CONTENTS

LIST OF FIGURES

CHAPTER I

INTRODUCTION

Preliminary Remarks

A sensitive method for detecting paramagnetic centers in solids is the use of electron spin resonance. Electron spin resonance (ESR)[1] can detect minute amounts of impurities or minute crystal defects because of the high sensitivity of the method. Electron spin resonance absorption can be observed only if an unpaired spin is associated with the defect or impurity. The unpaired electron interacts with an applied high frequency magnetic field producing transitions between Zeeman levels which are established by an external magnetic field. An unpaired electron can exist in a material for any one of several reasons. Donors and acceptors in semiconductors, color centers in the alkali halides, free radicals, and any crystal defect having an associated electron can exhibit ESR absorption (1, 2, 3).

---

[1] Electron spin resonance will be abbreviated as ESR when appropriate.

The purpose of the present study on diamond crystals which contain paramagnetic centers is to obtain information on the correlation of the diamond's color with its ESR absorption. The study will also include a brief review of the basic theory of ESR and a discussion of the equipment used in the investigation.

Electron Spin Resonance

The phenomena of ESR can be discussed by first considering a simple system in which an unpaired electron is associated with an atom or ion in a single crystal. At the present time only the interaction of the electron with the externally applied magnetic field will be considered. Relaxation, hyperfine interactions, spin-spin and spin-orbit interactions, and quadrupole interactions will be considered in some detail later. Before the external field is applied the energy levels of interest are degenerate. When the external field is applied each degenerate level will split into two levels, one with an energy above the original energy and one with an energy below the original. The interaction energy between the static field $\vec{H}$ and the magnetic moment of the electron $\vec{\mu}$ is $-\vec{\mu} \cdot \vec{H}$. The Hamiltonian for the system is of the form

$$[H] = -\vec{\mu} \cdot \vec{H}. \qquad (1.1)$$

For a static magnetic field applied in the z-direction the value of $\vec{H}$ is given by $\vec{H} = H_o \hat{k}$ and the Hamiltonian becomes

$$[H] = -\mu_z H_o. \tag{1.2}$$

When the value of μ_z is substituted in equation (1.2) where $\mu_z = -\gamma \hbar m_s$ equation (1.2) becomes

$$[H] = \gamma \hbar H_o m_s \tag{1.3}$$

where $\hbar$ is Planck's constant divided by 2π, m_s is the electron spin quantum number, $m_s \hbar$ is the component of the spin angular momentum in the direction of the applied magnetic field, and γ is the gyromagnetic ratio which is the ratio of the magnetic moment to the spin (a constant). When this value of the Hamiltonian is placed into Schroedinger's equation with $m_s = \pm \frac{1}{2}$ the energy levels of the unpaired electron are given by

$$E_{\pm} = \pm \tfrac{1}{2} \gamma \hbar H_o. \tag{1.4}$$

The energy splitting of the two levels is therefore given by

$$\Delta E = \gamma \hbar H_o. \tag{1.5}$$

A transition between the parallel and antiparallel Zeeman levels can be caused by an introduction of energy ΔE into the system, as will be discussed in greater detail in Chapter II. Since $\Delta E = \hbar \omega$, where ω is the angular frequency of the radiation energy, then using equation

(1.5) the conditions for a transition are met when

$$\omega_o = \gamma H_o. \tag{1.6}$$

Classically the magnetic moment vector precesses about the applied magnetic field direction with an angular frequency $\omega = \gamma H_o$ and the precession frequency is seen to correspond to the radiation energy frequency required to cause a transition between spin energy levels. This correspondence phenomena is known as resonance. It occurs at radiation frequencies in the x-band region of the microwave spectrum for field strengths of several kilogauss. To obtain a useful expression for this resonance condition in ESR, a new parameter (g) needs to be defined. The g-factor is the spectroscopic splitting factor given by

$$g = \frac{\gamma \hbar}{\beta} \tag{1.7}$$

where β is the Bohr magneton $\frac{\hbar}{2mc}$ (4). The expression for the resonance condition in ESR can now be obtained using (1.6) and (1.7) and is given by

$$h\nu = g\beta H \tag{1.8}$$

where $\nu = \frac{\omega}{2\pi}$ represents the microwave frequency.

Properties of Diamond

Diamonds have been classified into two principal types (5). Type I diamonds have an increasing ultra-

violet absorption coefficient for wavelengths shorter than 3000 A^{o} and infrared absorption bands in the 3-6μ and 6-13μ regions. Type II diamonds show the same 3-6μ absorption bands and these are believed to be due to lattice vibrational modes (6, 7). Type II diamonds do not absorb in the ultraviolet until a wavelength near 2200 A^{o} and show no absorption in the 6-13μ region of the infrared.

Type I diamonds have been broken down into a further classification based on their infrared absorption lines corresponding to different absorption centers (6, 7). Two of these centers have been designated group A and group B.

Group A

Infrared absorption bands: 7.0, 8.3, 9.1, and 20.8μ.

Ultraviolet: Cut-off moves to a longer wavelength and the intensity of the 3155 A^{o} line increases as the infrared absorption increases.

Group B

Infrared absorption bands: 7.0, 7.3, 7.5, 8.5, 10, 12.9, and 30.5μ.

Ultraviolet: The cut-off does not correlate with these band intensities.

Type II diamonds have also been broken down into a further classification. Their classification into Type IIa and Type IIb is based on their electrical conductivity

properties and other unusual characteristics such as special phosphoresences (6, 8, 9, 10). Type IIb diamonds are semiconductors and show absorption in the infrared at 1.85, 2.35, 2.43, 3.40, 3.56, 4.07 and 4.23 μ (7,11). They are usually blue in color (10); the blue being due to optical absorption in the red and near infrared (12). Type IIa diamonds do not possess these properties.

The differences in Type I and Type II diamonds have been partly attributed to a high concentration of nitrogen in Type I diamonds (13). Some concentrations as high as 0.2% have been reported. A linear relationship was found to exist between the concentration of nitrogen and the 7.8μ infrared absorption. These observations suggest that the nitrogen enters the diamond lattice substitutionally and gives rise to C-N molecular vibrations which cause the group A bands. No correlation has been observed between the group B bands and the nitrogen concentrations (14).

Other common impurities found in Type I diamonds are Si, Ca, Mg, Fe, Ti and Cu in concentrations as high as 10^{18} or 10^{19} atoms per cc. Type II diamonds both contain Si, Mg, and Al in concentrations of about 10^{15} atoms per cc. In general no direct correlation has been

found between the observed color or the optical and electrical properties of diamond and the type or amount of impurity known to be present.

Nitrogen has been detected in diamond using ESR methods and some important results of previous studies will be discussed in some detail later (15). These results contribute to the orientation methods used in the present study. Electron spin resonance has been detected in diamonds for various other defect centers and much work is still being done by workers in this laboratory as well as elsewhere. The exact nature of these structures has remained uncertain (16, 17, 18).

In conclusion, a good review of much of the previous research is contained in a study by King of this laboratory (19) and a text by R. Berman (20).

CHAPTER II

ELECTRON SPIN RESONANCE

Simple Theory

Solids with covalent or ionic bonds contain no unpaired spins and are diamagnetic but natural crystals contain defects caused by impurities and crystal lattice defects. These defects may have an unpaired spin associated with them which would make the solid paramagnetic.

In considering electron spin resonance the interaction of an electron spin system with an externally applied alternating magnetic system must be considered in more detail. The simple system previously considered will be referred to again here for clarity. Figure 1 shows the separation of the energy levels of an unpaired electron by a static magnetic field H_o as previously discussed in Chapter I.

The spin system is in thermal equilibrium before the microwave power is applied. The expression for the distribution of spins between the two levels is given by the Boltzmann expression

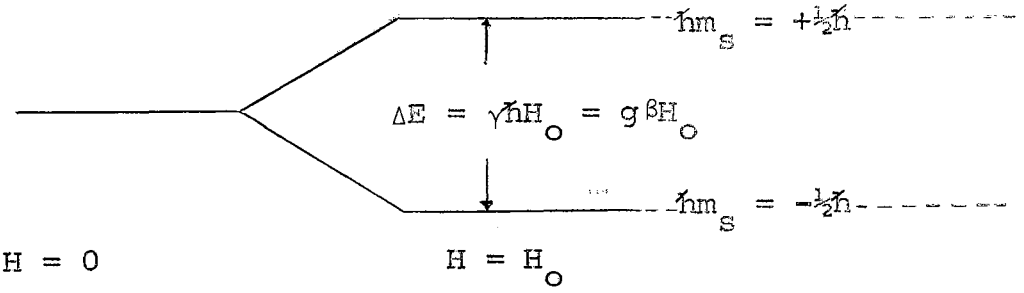

Figure 1. Separation of the energy levels of an unpaired electron by a static magnetic field H_o.

$$\frac{n+}{n-} = \exp - \frac{\Delta E}{kT} \qquad (2.1)$$

where n_+ is the number of spins in the upper level, n_- is the number in the lower level, T is the absolute temperature, and k is Boltzmann's constant. Equally populated levels result in just as many spins taking part in stimulated emission as there are in absorption and no net energy absorption occurs. A net absorption energy can occur under equilibrium conditions until the two levels become equally populated. Spin-lattice relaxation is one mechanism by which thermal equilibrium can be re-established. Coupling between the spin system and the lattice results in the spins losing energy to the lattice and thermal equilibrium is restored. Under these conditions a net absorption of energy from the microwave field can continue. The length of time required for

thermal equilibrium to be restored is known as "spin-lattice relaxation time". Weak coupling between the spin system and the lattice will result in a long relaxation time, whereas strong coupling produces short times. The phenomenon known as "saturation" occurs when weak coupling produces long relaxation times and a sufficiently high microwave power is introduced. Under these conditions thermal equilibrium cannot be completely restored by the coupling and the net absorption signal decreases or saturates.

When a nucleus possessing a magnetic moment is associated with the unpaired electron, the electron will see an internal field due to the magnetic moment of the nucleus. There will be an interaction between the unpaired electron and the nucleus, and the energy levels will split into several components depending upon the spin of the nucleus. For a nucleus of spin I there will be (2I+1) component levels and the ESR signal will have (2I+1) peaks. Figure 2 shows splitting of the levels for I=3/2. This hyperfine interaction makes it possible to identify the nucleus around which the electron is moving.

Rotating Coordinates and Resonance

The electron is considered to be a small magnet with

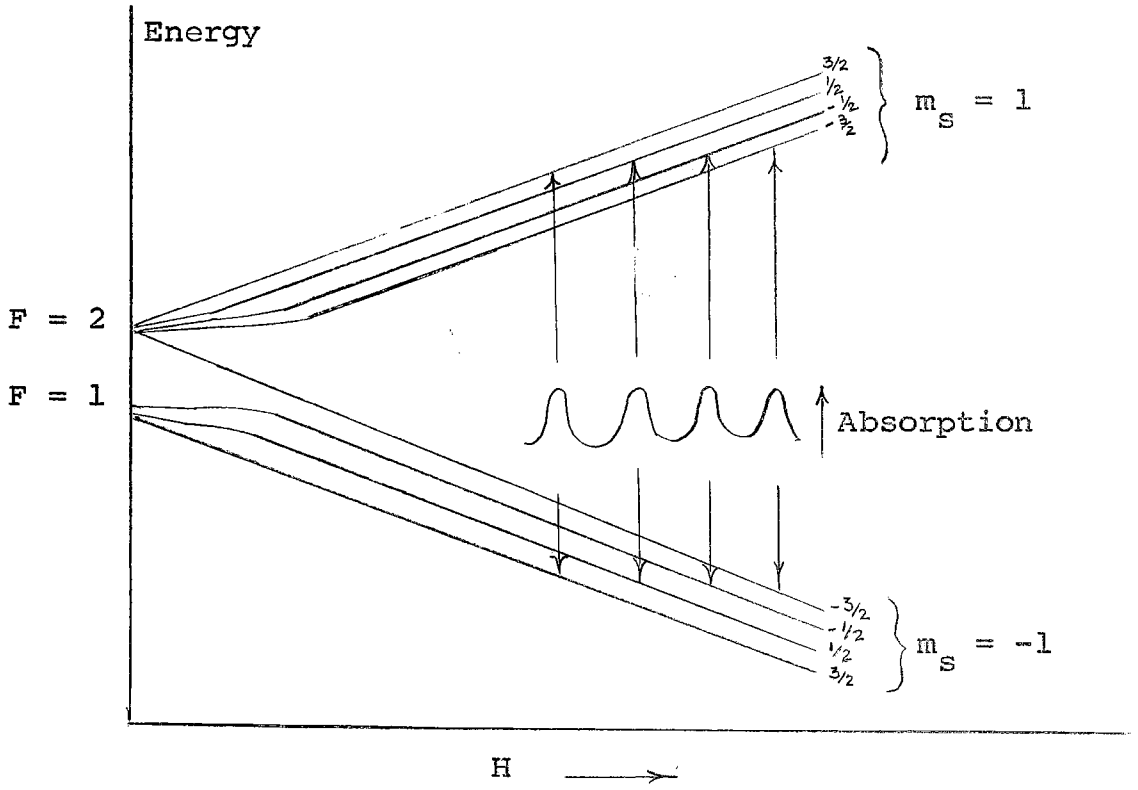

Figure 2. Electron spin resonance from an electron associated with a nucleus of spin I = 3/2.

magnetic moment $\vec{\mu}$ (21). In the presence of an external static magnetic field $\vec{H}$ the electron will experience a torque $\vec{T}$ given by

$$\vec{T} = \vec{\mu} \times \vec{H}. \qquad (2.2)$$

In the fixed laboratory system the z-axis of a rectangular coordinate system x, y, z is taken so that the static magnetic field is in the z-direction and is given by $\vec{H} = H_o \hat{k}$. The magnetic moment of the electron is related to the spin angular momentum by $\vec{\mu} = -\gamma \vec{S}$ where

$\vec{S} = \frac{3}{2}\hbar$. The equation of motion can then be obtained by noting that the time rate of change of angular momentum is just the torque $\vec{T}$ and is given by

$$\frac{d\vec{S}}{dt}. \tag{2.3}$$

This results in the following classical equation of motion in a fixed coordinate system:

$$\frac{d\vec{S}}{dt} = \gamma \vec{S} \times \vec{H}$$

and

$$\frac{d\vec{\mu}}{dt} = \vec{\mu} \times \gamma \vec{H}. \tag{2.4}$$

Since $\vec{\mu}$ cannot line up directly with $\vec{H}$, it will precess about $\vec{H}$ with a frequency $\vec{\omega} = \gamma H_o \hat{k}$, known as the Larmor frequency.

A solution to equation (2.4) can be obtained conveniently by transforming to a rotating coordinate system about the z-axis (22). The axes x' and y' rotate about the common z-axis with a constant angular frequency $\vec{\omega}$. An observer rotating with x' would see the time rate of change of $\vec{\mu}$ given by

$$\left(\frac{d\vec{\mu}}{dt}\right)_{rot}$$

and the rate of change due to the rotation of the axes would be given by

$$\vec{\omega} \times \vec{\mu}.$$

The equation of motion given in terms of the rotating system becomes

$$\frac{d\vec{\mu}}{dt} = \left(\frac{d\vec{\mu}}{dt}\right)_{rot} + (\vec{\omega} \times \vec{\mu}) \tag{2.5}$$

and solving for $\left(\frac{d\vec{\mu}}{dt}\right)_{rot}$ (2.5) becomes

$$\left(\frac{d\vec{\mu}}{dt}\right)_{rot} = \frac{d\vec{\mu}}{dt} - (\vec{\omega} \times \vec{\mu}).$$

Using equation (2.4) and rearranging gives

$$\left(\frac{d\vec{\mu}}{dt}\right)_{rot} = \gamma \left(\vec{H} - \frac{\vec{\omega}}{\gamma}\right) \times \vec{\mu}. \tag{2.6}$$

This is the equation for $\vec{\mu}$ in the rotating system. It has the same form as (2.4) except that $\vec{H}$ has been replaced by the effective field $\vec{H}_{eff}$, where $\vec{H}_{eff}$ is given by

$$\vec{H}_{eff} = \vec{H} - \frac{\vec{\omega}}{\gamma}. \tag{2.7}$$

If $\vec{\omega}$ is chosen such that $\vec{\omega} = \gamma H_o \hat{k}$ where $H_o \hat{k} = \vec{H}$ then $\left(\frac{d\vec{\mu}}{dt}\right)_{rot}$ will vanish. Therefore, when

$$\omega_o = \gamma H_o \tag{2.8}$$

where $\vec{\omega} = \omega_o \hat{k}$, the magnetic moment $\vec{\mu}$ is a constant vector and the magnetic moment precesses about $\vec{H}$ with a frequency $\omega_o = \gamma H_o$, the Larmor frequency. By comparing equation (2.8) with equation (1.6) it is seen that the Larmor precessional frequency is identical to the ESR absorption frequency.

The transformation just completed does not allow the

precession of the individual electron spins to be observed. Since the electron spin precesses about $\vec{H}$ at a constant frequency ω_o, an additional alternating magnetic field $\vec{H}_1$ must be introduced in the plane perpendicular to the static field $\vec{H}$ in order to cause spin-flip and allow resonance to be observed. The relative position of the field and the spin are shown in Figure 3c. The change of $\vec{S}$ is perpendicular to both $\vec{S}$ and H_o with angle θ being constant.

The alternating magnetic field $\vec{H}_1$ must be circularly polarized in the x and y plane and must have components

$$H_x = H_1 \cos \omega_1 t; \; H_y = H_1 \sin \omega_1 t \qquad (2.9)$$

where ω_1, is the microwave angular frequency. The component of $\vec{H}_1$ which is rotating in the same sense as $\vec{\mu}$ as the frequency approches the resonance condition is given by

$$H_{rot} = H_1 [\hat{i} \cos \omega_1 t + \hat{j} \sin \omega_1 t] \qquad (2.10)$$

where $\hat{i}$, $\hat{j}$, $\hat{k}$ are the unit vectors along x, y, z respectively. An additional torque is applied by $\vec{H}_{rot}$ in the z-direction, and the equation of motion (2.4) can be written

$$\frac{d\vec{\mu}}{dt} = \vec{\mu} \times \gamma [\vec{H} + \vec{H}_r]. \qquad (2.11)$$

A transformation to the rotating coordinate system

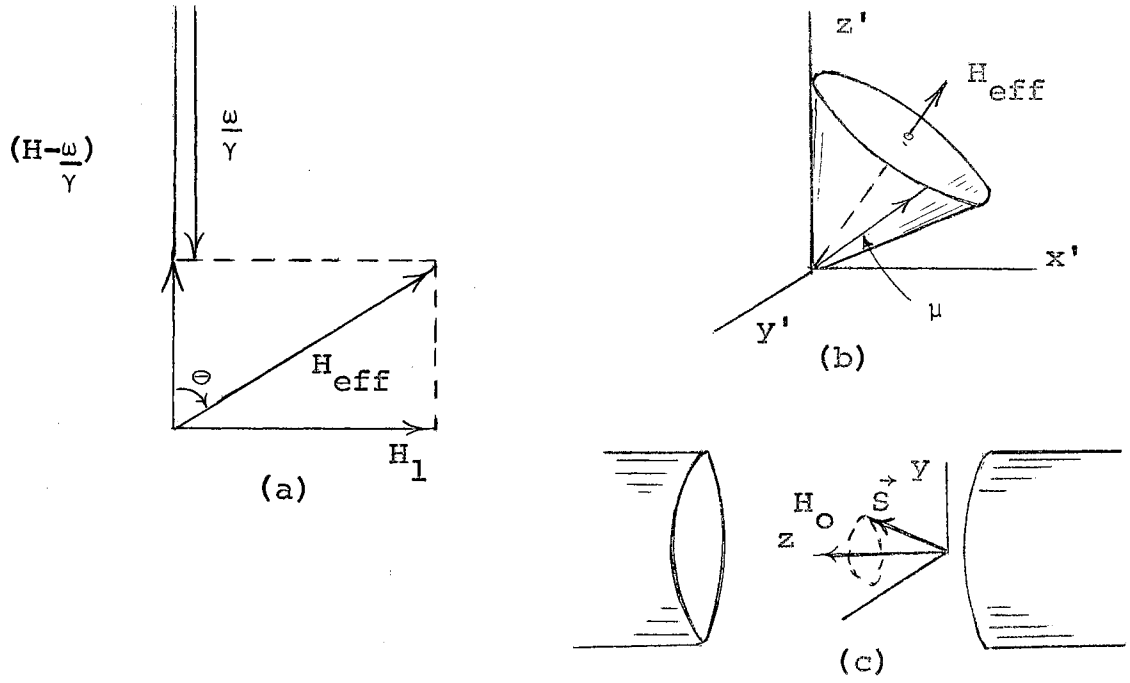

Figure 3. The Motion of the Magnetic Moment $\vec{\mu}$ in the effective magnetic field $\vec{H}_{eff}$ and the precession of $\vec{S}$ in the magnetic field H_o.

may also be used to treat the combined fields and equation (2.11) can be transformed to rotate with angular frequency $\vec{\omega} = \omega_1 \hat{k}$. Equation (2.11) in the rotating system is given by

$$\left(\frac{d\vec{\mu}}{dt}\right)_{rot} = \vec{\mu} \times \gamma \left[\left(H_o - \frac{\omega}{\gamma}\right) \hat{k} + H_1 \hat{i}' \right] \qquad (2.12)$$

where $\vec{H}_r$ is a constant in the xy-plane directed along the x-axis as shown in Figure 3a and $\vec{H}_r$ is given by $\vec{H}_r = H_1 \hat{i}'$. The effective field, as seen from the rotating system, acts as a constant field. The magnetic moment precesses, as shown in Figure 3b, about $\vec{H}_{eff}$ in a cone at frequency

$\vec{\omega}_{eff} = \gamma \vec{H}_{eff}$ where $\vec{H}_{eff}$ is given by

$$\vec{H}_{eff} = H_1 \hat{i}' + (H_o - \frac{\omega_1}{\gamma})\hat{k}'. \qquad (2.13)$$

When the microwave frequency ω_1 is at the resonance condition the effective field is $H_1\hat{i}'$ and $\vec{\mu}$ precesses about $\vec{H}_1$ with a frequency $\vec{\omega}_p = \gamma\vec{H}_1$. The magnetic moment of the electron in the rotating system is

$$\vec{\mu} = [\mu_x \hat{k}' \cos \omega_p t - \mu_y \hat{j}' \sin \omega_p t] \qquad (2.14)$$

where $\vec{\mu}$ precesses in a plane perpendicular to $\vec{H}_{eff}$ and changes its orientation periodically. The orientation of $\vec{\mu}$ changes from parallel to antiparallel with respect to the static field $\vec{H}$ with a frequency $\omega_p << \omega_o$ which causes a slow tipping of $\vec{\mu}$ as it rapidly precesses around $H_o >> H_1$.

Bloch Equations

The previous discussion did not include equilibrium conditions caused by relaxation effects. After application of the static magnetic field in the z-direction, before any energy is introduced into the system the electrons will align themselves parallel or antiparallel to the field as previously stated. At thermal equilibrium the spins populate the two levels approximately with a Boltzmann distribution and there is a resulting magnetization $M_o\hat{k}$, which is given by

$$M_o\hat{k} = \chi_o H_o \hat{k} \qquad (2.15)$$

where χ_o is the static magnetic susceptibility. The rate of change of the x, y and z components of the magnetization as the system approches equilibrium are given by Bloch (23) to be

$$\frac{dM_x}{dt} = M_x = -\frac{M_x}{T_2} \qquad \text{(a)}$$

$$\dot{M}_y = -\frac{M_y}{T_2}, \qquad \text{(b)} \qquad (2.16)$$

$$\dot{M}_z = -\frac{(M_z - M_o)}{T_1} \qquad \text{(c)}$$

where T_2 is the "spin-spin relaxation time" in the transverse x and y directions, and T_1 is the "spin-lattice relaxation time" in the longitudinal z direction. Equations (2.16 a, b, c) are known as the Bloch equations.

The equation of motion without the relaxation effects was previously given as

$$\frac{d\vec{M}}{dt} = \gamma \vec{H} \times \vec{M}. \qquad (2.4)$$

When relaxation effects are included, and assuming $H_1 << H_o$, equation (2.4) becomes

$$\frac{d\vec{M}}{dt} = \gamma \vec{H} \times \vec{M} - \frac{M_x \hat{i} + M_y \hat{j}}{T_2} - \frac{M_z - M_o}{T_1} \hat{k} \qquad (2.17)$$

which transforms into the rotating system as

$$\left(\frac{d\vec{m}}{dt}\right)_{rot} = \gamma(\vec{H}_e \times \vec{M}) + \frac{M_o - M_{z'}}{T_1}\hat{k}' - \frac{M_{x'}}{T_2}\hat{i}' - \frac{M_{y'}}{T_2}\hat{j}' \quad (2.18)$$

When the substitutions $\vec{H}_e = (H_o + \frac{\omega}{\gamma})\hat{k}' + H_1\hat{i}'$, $\omega_o = -\gamma H_o$, and $\omega_1 = -\gamma H_1$ are made into equation (2.18) it may be solved and simplified to give

$$\dot{M}_{x'} = -M_{y'}(\omega_o - \omega) - \frac{M_{x'}}{T_2}, \quad (a)$$

$$\dot{M}_{y'} = -M_{z'}\omega_1 + M_{x'}(\omega_o - \omega) - \frac{M_{y'}}{T_2}, \quad (b) \quad (2.19)$$

$$\dot{M}_{z'} = M_{y'}\omega_1 + \frac{M_o - M_{z'}}{T_1}. \quad (c)$$

If the rate at which H_o is swept through resonance is long compared to the relaxation time, the magnetization can be assumed to maintain its equilibrium value, and to a first approximation

$$\dot{M}_{x'} = \dot{M}_{y'} = \dot{M}_{z'} = 0.$$

Assuming a weak alternating field $\vec{H}_1$ so that $T_1T_2\omega_1^2 \ll 1$, the equations (2.19 a, b, c) may be solved and simplified to give equations (2.20 a, b, c) as shown on the following page. The solutions to these equations are obtained using an approximation utilizing slow passage because this condition relates the scanning rate to the relaxation times. When this is done equation (2.19) becomes

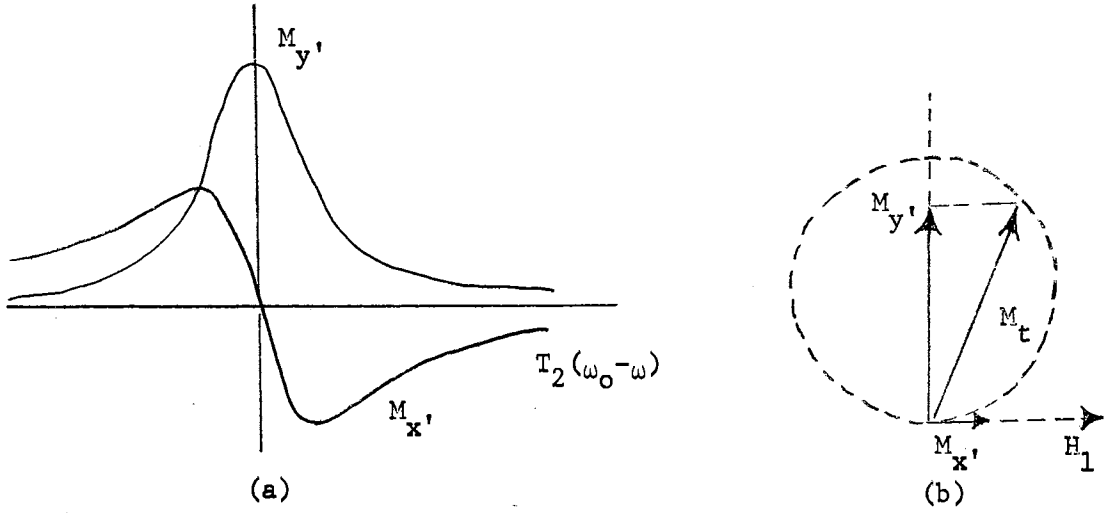

Figure 4. Transverse magnetization; (a) dispersive and absorptive modes, (b) vector relationship in a rotating frame.

$$M_{x'} = \frac{M_o T_2^2 \omega_1 (\omega_o - \omega)}{1 + T_2^2 (\omega_o - \omega)^2}, \qquad \text{(a)}$$

$$M_{y'} = -\frac{M_o T_2 \omega_1}{1 + T_2^2 (\omega_o - \omega)^2} \qquad \text{(b)} \quad (2.20)$$

$$M_{z'} = M_o. \qquad \text{(c)}$$

The equations (2.20 a, b) can be graphed, yielding $M_{x'}$ and $M_{y'}$ as functions of $T_2(\omega_o-\omega)$ as in Figure 4a. Such a plot shows the curves as representations of the dispersive and absorptive modes of a harmonic oscillator. The transverse magnetization vector $\vec{M}_t$ is found to move in a circle as shown in Figure 4b. At resonance $\vec{M}_t$ is shifted from $\vec{H}_1$ by 90^o and is equal to $\vec{M}_{y'}$ maximum.

If the high frequency susceptibility χ is now introduced where χ is given by

$$\chi = \chi' - i\chi'', \tag{2.21}$$

and M_x is taken as the real part of $\chi\,[2H_1 \exp(i\omega t)]$ then M_x is given by

$$M_x = \chi' 2H_1 \cos\omega t + \chi'' 2H_1 \sin\omega t. \tag{2.22}$$

Consideration of the components of $M_{x'}$ and $M_{y'}$ in the x-direction allow M_x to be written in the form

$$M_x = M_{x'} \cos\omega t - M_{y'} \sin\omega t. \tag{2.21}$$

Comparing equations (2.22) and (2.21) shows that

$$\chi' = \frac{M_{x'}}{2H_1}, \qquad \chi'' = -\frac{M_{y'}}{2H_1} \tag{2.22}$$

where χ' gives the dispersion curve and χ'' gives the absorptive curve.

It should be noted that the power absorbed from the alternating field depends on χ'' and is given by

$$P = 2\omega H_1^2 \chi''$$

so that

$$P = \chi \cdot \omega \frac{T_2 \omega_o H_1^2}{[1 + T_2^2(\omega_o - \omega)^2]}$$

$$= \pi \chi_o \omega \omega_o H_1^2 L(\omega) \tag{2.23}$$

where

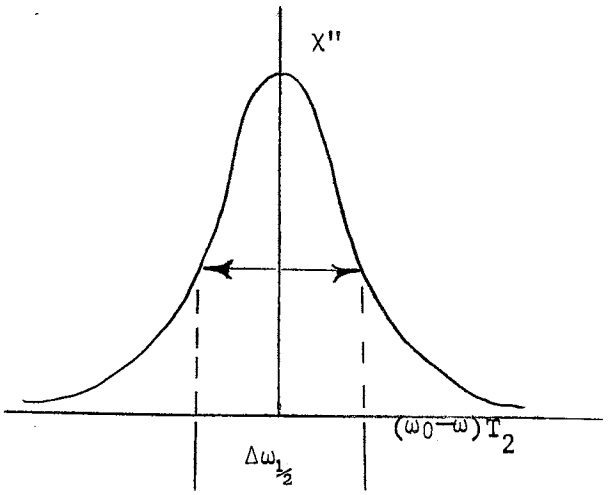

Figure 5. The Lorentzian line shape for $\chi"$.

$$L(\omega) = \frac{T_2}{\pi}\left[\frac{1}{1 + T_2^{\,2}(\omega_o - \omega)^2}\right]$$

is the Lorentzian line shape as shown in Figure 5. Note that the width of the resonance line at half intensity is given by

$$\Delta\omega_{\frac{1}{2}} = 2(\omega_o - \omega) = \frac{2}{T_2} \quad . \tag{2.24}$$

In terms of units of magnetic field (2.24) can be written as

$$\Delta H = \frac{2}{\gamma T_2} \quad . \tag{2.25}$$

To obtain a more detailed discussion of the Bloch method refer to the book by Abragam (24).

CHAPTER III

INSTRUMENTATION

Basic ESR Spectrometer

Many ESR spectrometers operate in the x-band region of the microwave spectrum which is in the 3cm wavelength range and corresponds to a frequency of about 9.5gHz. The condition for resonance is given by

$$E = h\nu = g\,\beta H \qquad (3.1)$$

where g for free electrons is approximately 2 (25). When this value of g is substituted into (3.1) along with the values of h, ν, and β, as previously discussed, a value of magnetic field, H, is obtained which is approximately 3,400 gauss. A magnetic field of approximately 3,400 gauss is therefore required to produce free electron resonance in the region of the microwave spectrum.

There are two common types of electron spin resonance spectrometers; one form uses a reflection cavity, the other a transmission cavity. The reflection cavity offers the most versatility and is used most often when a bridge spectrometer is employed. Since the spectrometer used in

this study utilizes a reflection cavity, only this type will be discussed. To detect ESR the sample is placed in the cavity in the magnetic field of an electromagnet. Since it is inconvenient to vary the microwave frequency, the magnetic field is scanned so that the resonance condition (3.1) is satisfied. The field configuration of the cavity must be selected to place the microwave magnetic field perpendicular to the electromagnet field at the position of the sample in the cavity. When the resonance condition is satisfied energy will be absorbed from the microwave field and detected by additional instrumentation.

The electron spin resonance spectrometer consist of several basic components as shown in Figure 6. The components are as follows:

(1) An electromagnet and magnet power supply with a method by which the field can be swept linearly through the resonance line.

(2) A modulation system that introduces a small alternating component to the sweep of the magnetic field and provides a reference voltage for the phase-sensitive detector used in the detection system.

(3) A sample cavity in which the sample is placed.

(4) A microwave circuit that introduces microwave energy into the cavity and permits monitoring of the

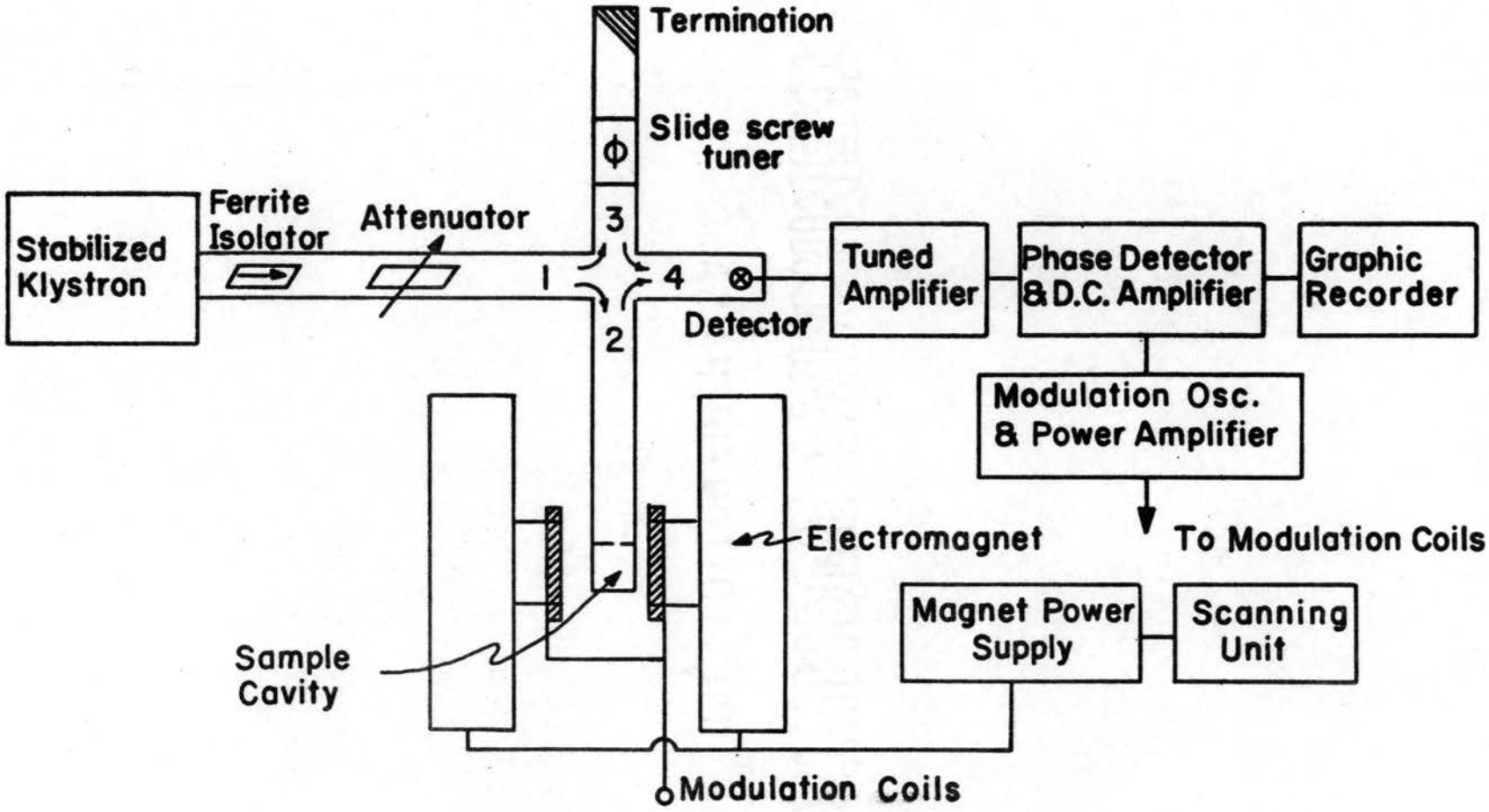

Figure 6. Basic components of an ESR bridge spectrometer. (After Bell ($_{26}$).)

reflected energy.

(5) A source of microwave energy that is frequency stabilized and has a power output near 100 milliwatts.

(6) An ESR signal amplifier and a phase-sensitive detector operating at the modulation frequency.

(7) A graphic recorder or oscilloscope which records the output of the phase-sensitive detector.

These basic components are usually used in one form or another though they may be modified. Additional components are usually included which increase stability and signal-to-noise ratio for increased sensitivity.

Description of the Spectrometer Used in this Study

The spectrometer used in this research was constructd mainly by Bell of this laboratory using fundamental ESR design techniques (26). It is a microwave bridge spectrometer which utilizes a reflection cavity and consist of many of the components previously discussed. The complete spectrometer used in this research is shown in Figure 7 and a brief discussion of the functions of the different components will be given.

The Electromagnet

The magnet system is the most expensive single system

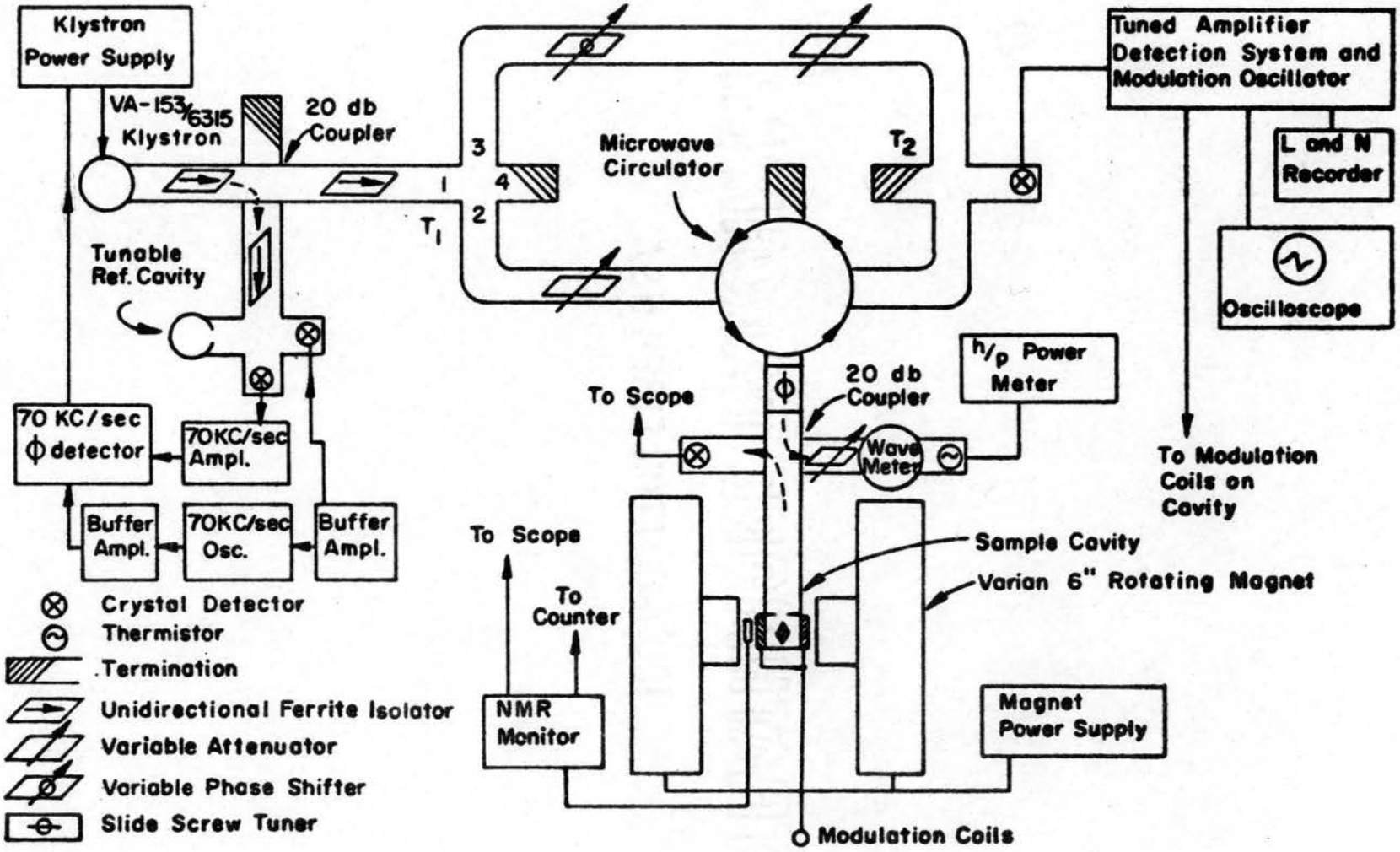

Figure 7. Electron spin resonance spectrometer used in the study. (After King (19).)

in the spectrometer and usually must be chosen from an economic viewpoint; however, an x-band ESR spectrometer must have a homogeneity of better than 0.1 gauss in $1cm^3$ and these minimum requirements must be met (2). The pole gap must be large enough to accomodate the cavity and all necessary accessories. Although it would be advantageous to have a very large gap and high homogeneity, the cost of these features must be considered. A practical median between cost and quality should determine the type of magnet to be used.

The magnet used in the study is a Varian 6" electromagnet, Model 4007-1. It can be turned through 200^{o} about the vertical axis and has 6" ring shim pole pieces with a 2.875" gap. A Model V-2200 Varian regulated power supply is used with the magnet. The magnetic field contours produced by the 6" pole pieces with a 2.875" gap are shown in Figure 8.

The scan rate of the field and the contours of the field are measured using a nuclear magnetic resonance detector. The detector probe is supported by a clamp around one of the magnetic pole pieces and the frequency of the nuclear magnetic resonance oscillator is measured with a h/p 524 D electronic counter. The frequency of the oscillator is related to the proton resonance and the

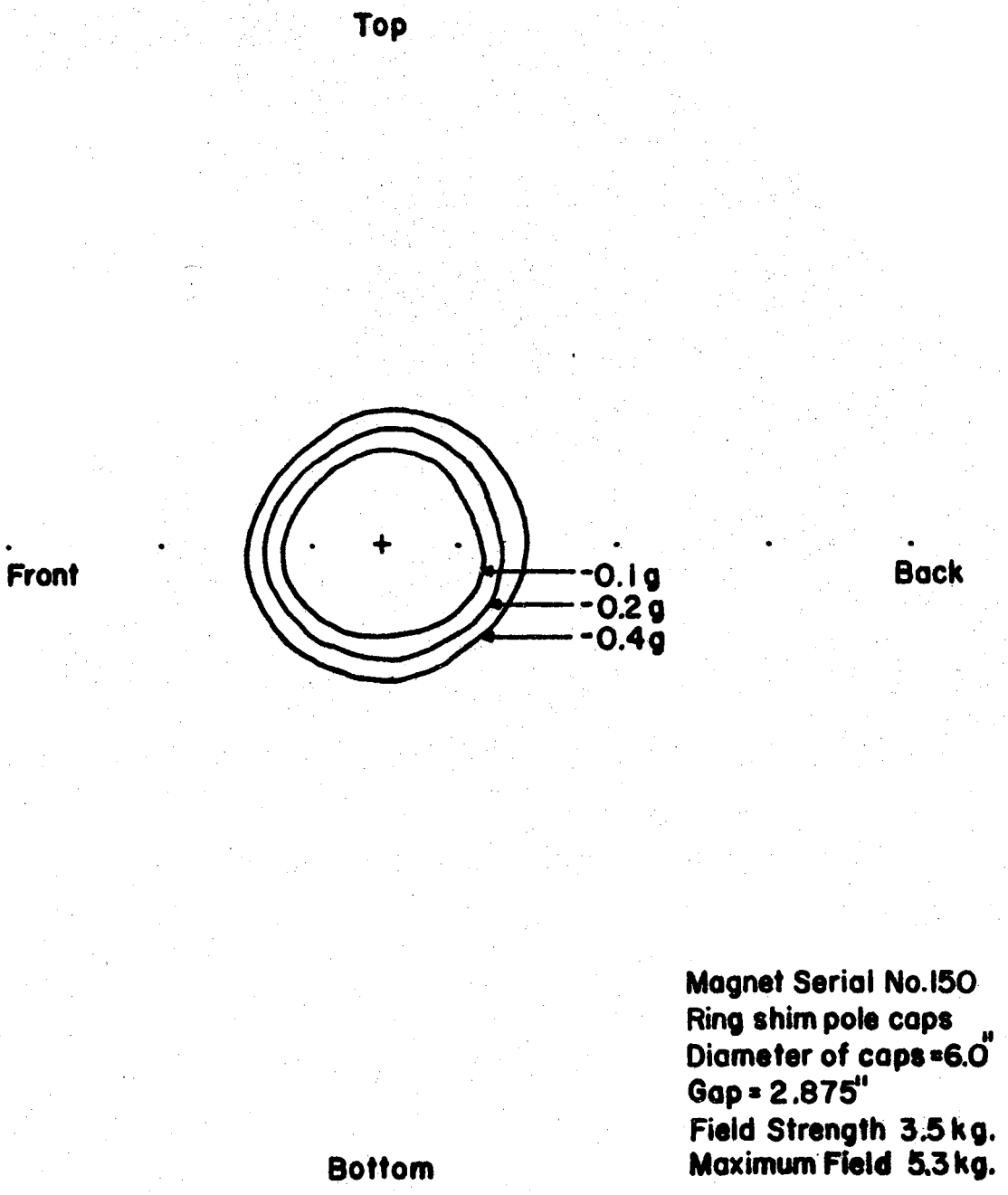

Figure 8. Magnetic field plot of Varian Model V4007-1 electromagnet. (After King (19).)

relationship between this frequency and the magnetic field is given by

$$H = \frac{2\pi}{\gamma_p} \nu_p = 2.34868 \times 10^4 \nu_p \qquad (3.2)$$

where $\gamma_p = 2.67530 \times 10^4$ radian sec.$^{-1}$ gauss^{-1} is the gyromagnetic ratio of the proton (27).

Modulation System

In order to avoid the instability of the dc amplifiers the field is usually modulated so that ac amplifiers may be used. The modulation coils may be placed on the pole pieces, on the sides of the cavity, or inside the cavity. The modulation amplitude should be variable so that very small as well as very large modulating fields are available allowing maximum sensitivity for the line width and shape of the ESR lines to be studied. The maximum sensitivity is obtained when the peak to peak modulation amplitude is on the order of the line width of the ESR signal, but distortion occurs if the modulation amplitude exceeds 1/10 of the line width (2).

Although a low frequency modulation system with bolometers used as detectors is available for use with the spectrometer, a 100kc modulation system was used exclusively (26). The system consist of a pair of modulation

coils mounted on the cavity walls, so that the modulation field is parallel to the large dc magnetic field, and a Varian 100kc modulation control unit containing a tuned amplifier, a phase detector, a crystal oscillator, and a modulation amplifier.

Several effects must be considered when choosing the frequency of modulation to be used. When a crystal detector is used to detect the ESR signal the crystal noise voltage is proportional to $(f)^{-\frac{1}{2}}$ and the crystal noise power varies as $\Delta f/f$, where Δf is the band width of the modulation frequency f. This means that at some low frequency, 100cps for instance, the noise voltage is $(f/100)^{\frac{1}{2}}$ times that at f. Therefore, at 100kc the noise voltage is approximately 1/30 that at 100cps for the same band width. Bolometers do not have the f^{-1} dependence and can be used as detectors at very low frequencies without serious noise problems. It would seem that, if crystal detectors are to be used, a very high modulation frequency would be most desireable. However, for frequencies much higher than 100kc other problems begin to appear. At extremely high modulation frequencies the walls of the cavity begin to attenuate the signal and the large modulation amplitudes needed at the sample are hard to obtain. Even at 100kc the walls of the cavity must be metallic

plated glass or ceramic. If higher frequencies are to be used the modulation must be introduced directly into the cavity by the use of a high frequency loop rigidly connected and inserted properly into the cavity.

Sample Cavity

The sample cavity is one of the most important components of a microwave spectrometer and special cavity designs are necessary for measurements under particular conditions. The choice between several cavity structures is determined by the space available in the magnet gap, the size and shape of the sample, the necessary Q for the cavity, the desired microwave magnetic field configuration at the sample, and the special effects which are to be observed. Two of these several cavity structures are shown in Figure 9. The sample is placed in the position of maximum microwave magnetic field and minimum microwave electric field.

The Varian V-4531 rectangular ESR cavity (Figure 9a), operating in the TE_{102} mode, is the only cavity used in the present study. It is equipped with varible temperature capabilities from -185°C to 300°C, but all data taken in this study was at room temperature and these capabilities were not used. The rectangular cavity has the

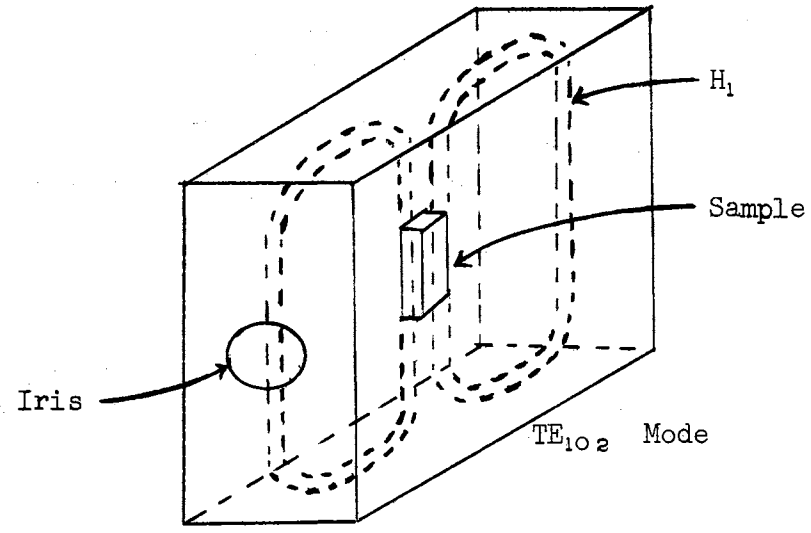

(a)

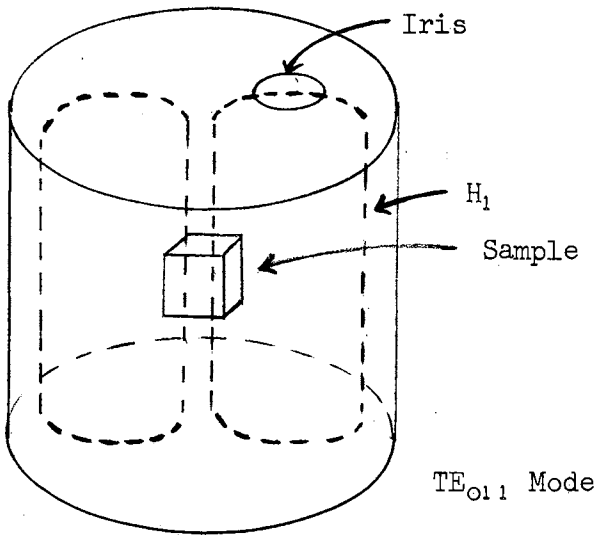

(b)

Figure 9. Sample cavities showing microwave magnetic field and location of sample. **(After King (19).)**

disadvantage that the microwave magnetic field is introduced in the horizontal plane when placed in the magnet gap and the rotatable magnet cannot be moved. If rotation is necessary the sample must be rotated by turning the quartz rod that suspends the sample in the middle of the cavity.

The cavity is coupled to the waveguide by means of a variable dielectric coupling scheme (28,29). The cavity is not adjusted for critical coupling but is adjusted so that the cavity is slightly undercoupled. If critical coupling were used the possibility of mixing the absorptive and dispersive modes would be present; this is an undesirable situation.

The Microwave Circuit

The microwave bridge and circuit is shown in Figure 7. Its basic function is to introduce the microwave energy into the cavity and permit monitoring of the reflected energy (30). The power from the klystron is divided by a magic Tee (T_1) and travels into the upper and lower branches of the circuit. The power down arm 2 is introduced into the circulator after passing through a Varian adjustable precision attenuator. The attenuator controls the amount of energy incident on the sample in

the cavity. The power entering arm 1 of the circulator must exit by arm 2 and is coupled to the cavity (31). The power reflected from the cavity enters the circulator at arm 2 and must exit from arm 3 into magic Tee (T_2). Half the power is detected by the crystal detector in arm 2 of T_2 and the other half is dissipated in arm 3 of T_2. A small amount of power is coupled from the cavity arm into a 20 db coupler and is detected by a crystal detector. The detected signal feeds a wavemeter, a power meter, and an oscilloscope.

The power that travels up through arm 3 of T_1 is used to bias the crystal detector. This arm contains a ferrite isolator, an adjustable phase shifter, and an adjustable attenuator. The phase shifter and the attenuator control the bias on the crystal detector. The energy in this arm enters the magic Tee (T_2) by the upper arm and travels into arm 2 and 3 of T_2. The bias attenuator maintains the desired bias voltage on the detector and the bias phase shifter controls the phase of the bias voltage. These controls determine whether the bridge is sensitive to dispersive (χ'), or the absorptive (χ'') component of the magnetic susceptibility.

The slide screw tuner in the cavity arm is adjusted so that the reflected power from the cavity is independent

of the incident power to the cavity and the bridge is balanced so that no reflected power reaches the detector arm until the sample resonance is reached. A suitable adjustment of the phase shifter will enable the desired mode of operation to be selected. By proper adjustment of the reference voltage to be sensitive to either amplitude or phase unbalance, the desired component can be obtained (28,32).

Stablized Klystron

The microwave energy is supplied by a Varian reflex klystron, VA 201B, which produces approximately 100 milliwatts of power. A commercial klystron power supply is used as the source of power to the klystron and the klystron is mounted on vibration free supports. The entire klystron is thermally isolated in a water cooled silicone oil bath.

It is necessary to keep the klystron frequency stable over at least the entire period of time required to record the passage through resonance. Stablization increases the signal-to-noise ratio and helps prevent the admixture of the real (χ') and imaginary (χ'') parts of the magnetic susceptibility with a great simplification of the recorded data. The stabilization system used in the present study

is the modified Pound circuit shown in Figure 10 (33, 34, 35, 36).

A small part of the microwave power from the klystron is coupled through a 20 db coupler into arm 1 of the magic Tee shown in Figure 10 and Figure 7. The power divides into arm 2 and 3 which are adjustable to be of equal effective lengths. Arm 3 is a matched load, and there is no reflected power if the 70kc modulation is not present. When modulation voltage is present the signal that enters arm 3 is mixed with 70kc signal at the crystal. The crystal superimposes the 70kc frequency and the microwave frequency to produce side bands 70kc above and 70kc below the klystron frequency. When the reference cavity is critically coupled, there is no reflected energy from arm 2 if the klystron frequency coincides with the reference cavity resonance frequency. If the frequencies do not coincide, the reflected wave from the cavity has a magnitude dependent upon the frequency difference.

At the crystal detector in arm 4 the three signals come together and are mixed at the detector giving a 70kc signal proportional to the reactive part of the wave reflected from the cavity. There is a 180° phase difference on either side of the cavity resonance, and

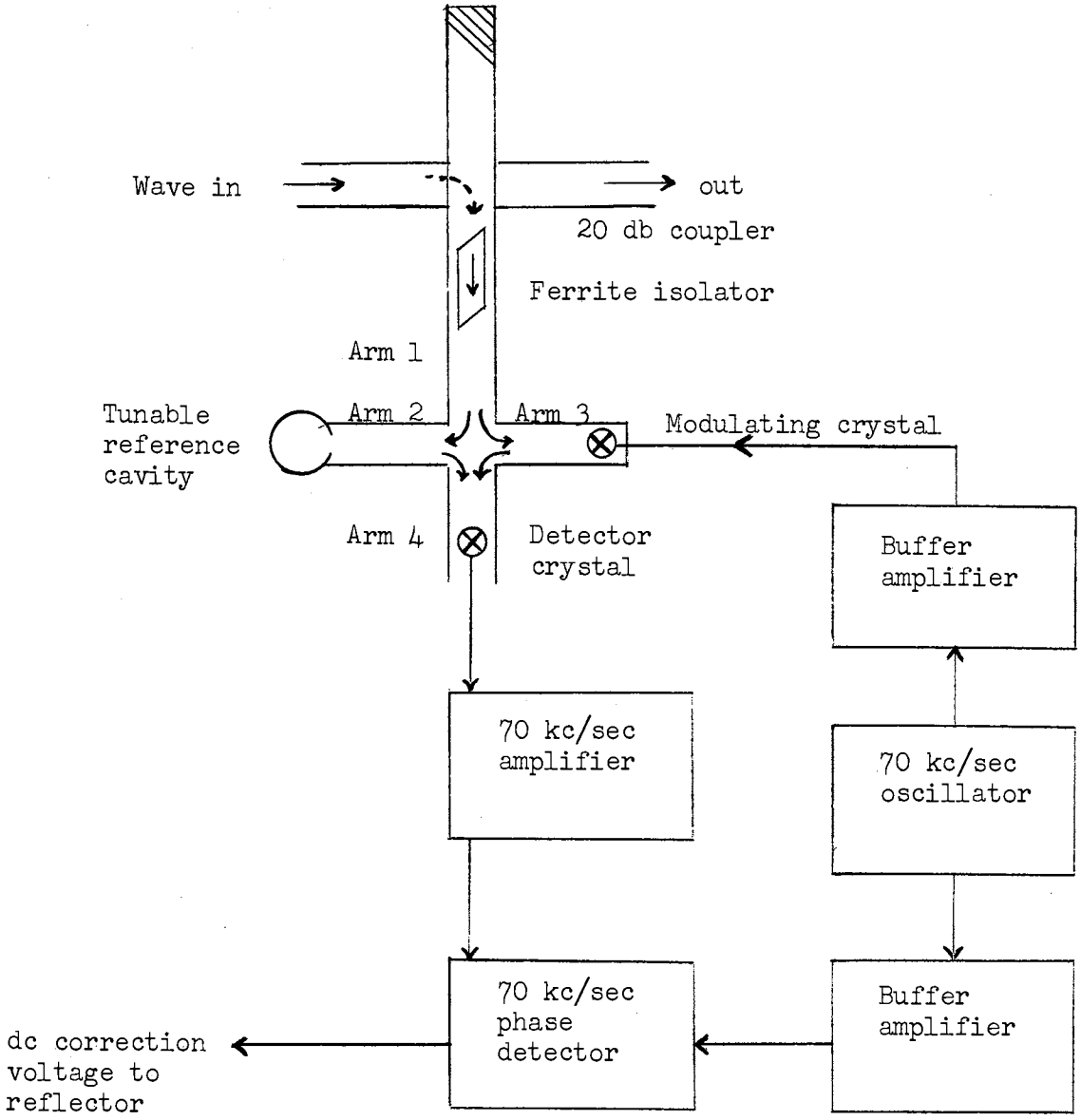

Figure 10. Modified Pound frequency stabilizer.
(After King (19).)

the deviation of the klystron on either side of resonance will affect the phase of the crystal output (30). The 70kc error signal is amplified, demodulated, and compared with the reference phase signal in the phase detector. The output of the phase detector is a ±dc signal with an amplitude determined by the error signal strength and a sign determined by the error signal phase. The error signal is amplified and applied to the klystron reflector to adjust the klystron frequency. Since the reflector of the klystron operates at high negative potentials, the phase detector cannot be grounded and must be carefully isolated from ground. The frequency of the klystron is now regulated, or locked, to the resonant frequency of the reference cavity which can be manually set to a desired frequency by moving the cavity bottom plate as shown in Figure 11.

Signal Detection and Display

When the bridge is adjusted for the absorptive mode the incident waves on the crystal detector in arm 2 of Tee (T_2) are the bias signal and the amplitude modulated reflected signal from the sample cavity. These signals are mixed at the detector and sent to the Varian modulation and control unit as shown in Figure 7.

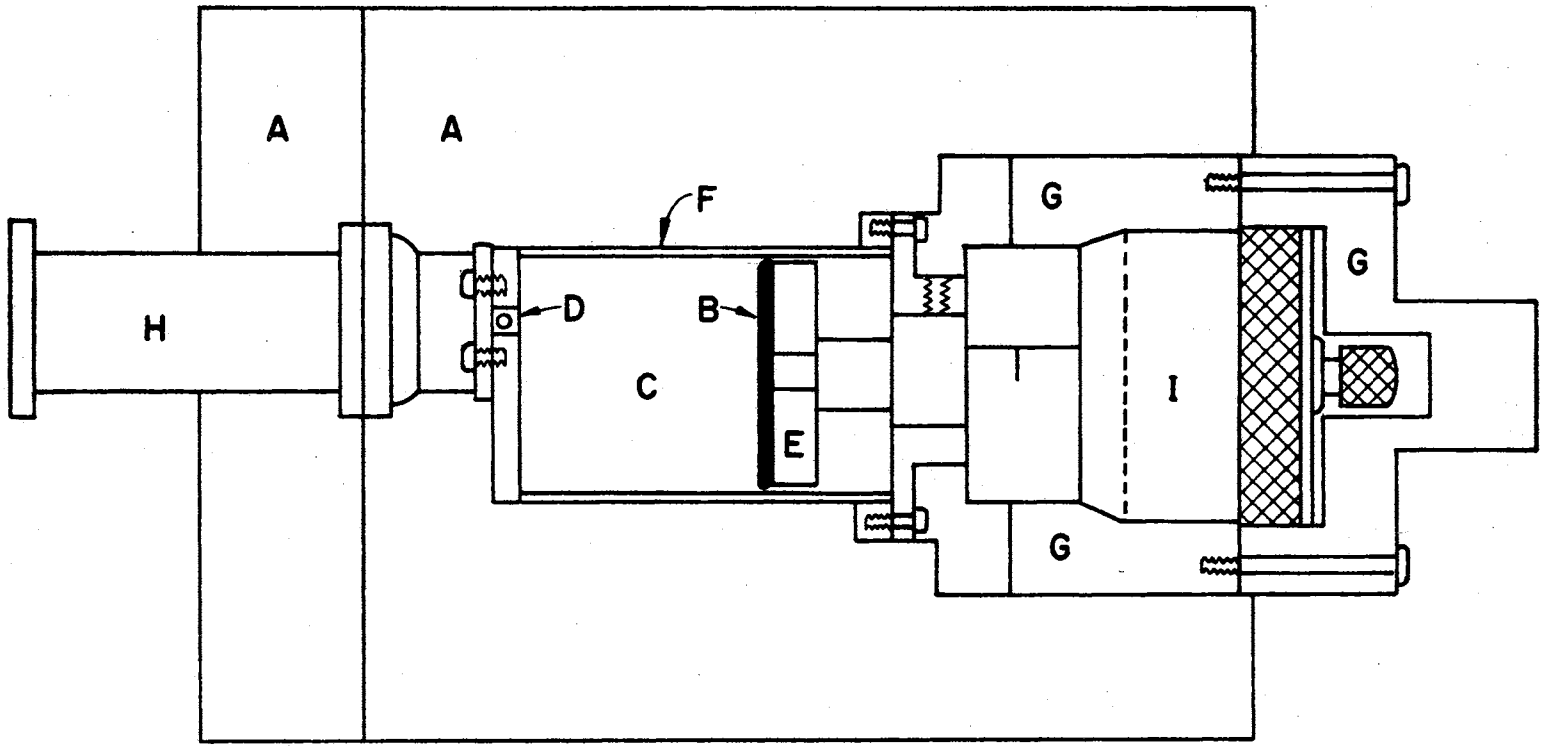

A — Styrofoam Insulation
B — Moveable Cavity Bottom Plate
C — Resonance Cavity
D — Iris and Coupling Screw
E — Eccosorb Epoxy
G — Plexiglas
H — Waveguide
I — Micrometer

F - Silver Plated Quartz Cylinder

Figure 11. Cylindrical reference cavity. (After King (19).)

The components of the Varian control unit have been described previously but will be mentioned again for the sake of clarity. The unit consist of a 100kc crystal oscillator which acts as a reference for the phase detector and provides 100kc modulation to the modulation coils, a 100kc amplifier and demodulator, and a rectification integration circuit from which the signal is sent to the graphic recorder for display.

The phase detector locks onto the input signal which is a continuous vector sum of the amplitude modulated signal voltage and the bias voltage. The detector output can be operated with respect to the phase of the reference signal either in phase or in varying degrees of phase displacement from the reference voltage. In the present study only in-phase and 90^{o} displacement was utilized. The signal output of the detector system is the first derivative of the actual absorption line. It is sent to the integrator circuit and then to the graphic recorder.

If low frequency modulation is desired, the twin bolometers (barretters) available with the spectrometer can be used as detectors. Bolometers respond only to changes on the order of one millisecond (37). They are used with modulation frequencies of 28,400 and 1,000cps

and a phase detector with a range from zero to 1,800cps produced by using a Bristol synchroverter (26). The bolometers contain a wire filament which changes resistance as the microwave energy incident upon it changes and a low-noise amplifier is used in connection with the bolometer bridge.

CHAPTER IV

RESULTS AND DISCUSSION

General Remarks

Remarks on Experimental Observations

The electron spin resonance spectra of a large number of Type I (insulating) diamonds were studied. In particular, the correlation between the color of each diamond and its related ESR spectrum was investigated. The diamonds were classified into groups according to their actual color and two or three of these diamonds were compared within their group to see if the similarity in color caused a similarity in ESR spectra. The splitting, the position, and the number of complex peaks were used as the methods of comparison. All of the Type I diamonds used in the investigation displayed strong substitutional nitrogen resonance signals and all had g values of approximately 2. In addition to the diamonds actually used in the experimentation, data previously taken by workers on other diamonds was used in the comparisons. No semicon-

ducting diamonds were used by this investigator but comparison of previous data was used for correlation of blue diamonds. All new data, and all that used as a comparison, was taken at room temperature.

A description of the diamonds used will be given as each group is discussed.

Orientation Procedure

The diamonds were oriented using a Laue back-reflection x-ray camera. They were mounted on a goniometer with beeswax and irradiated with x-rays. A Greninger chart was used to obtained the desired rotations for proper orientation. After the rotations were made a second x-ray picture was taken, and any further rotations necessary for exact orientation were made. This process was repeated until the desired orientation was achieved exactly. The diamonds were then transferred to a quartz sample-holder rod which was clamped securely parallel to the diamond's orientation direction. The diamond was then glued to the quartz rod and removed from the beeswax.

The orientation was checked after the sample was placed in the rectangular Varian sample cavity of the ESR spectrometer. All the samples displayed a strong nitrogen resonance, and the orientation could be checked

by noting the exact shape and number of nitrogen side peaks following the study by Smith, et al., (15). In this study the nitrogen was assumed to occupy a substitutional lattice position with the unpaired electron forming a hybridized sp^3 antibonding orbital along one of the C-N bonds. The electron was assumed to be localized on any of the $\langle 111 \rangle$ bonding directions. When $\vec{H}$ is parallel to one of the $\langle 100 \rangle$ directions, (2I + 1) hyperfine lines will be produced. Nitrogen has a spin I=1 which produces a hyperfine structure of three peaks with ratios of 1 : 1 : 1. For arbitrary orientations with respect to the $\langle 100 \rangle$ directions the side peaks split up into as many as four peaks. The side peaks splitting for the major directions is shown in Figure 12.

Data Presentation

The actual recorder graphs could not be photographed directly because of the color of ink used in the recorder pen. Therefore, it was necessary to trace the actual graphic representations as accurately as possible and use these tracings for comparison purposes. Since it was desirable to include actual copies of the recorder graphs showing all noise and exact signal ratios, these were Xeroxed individually and appear in Appendix A of

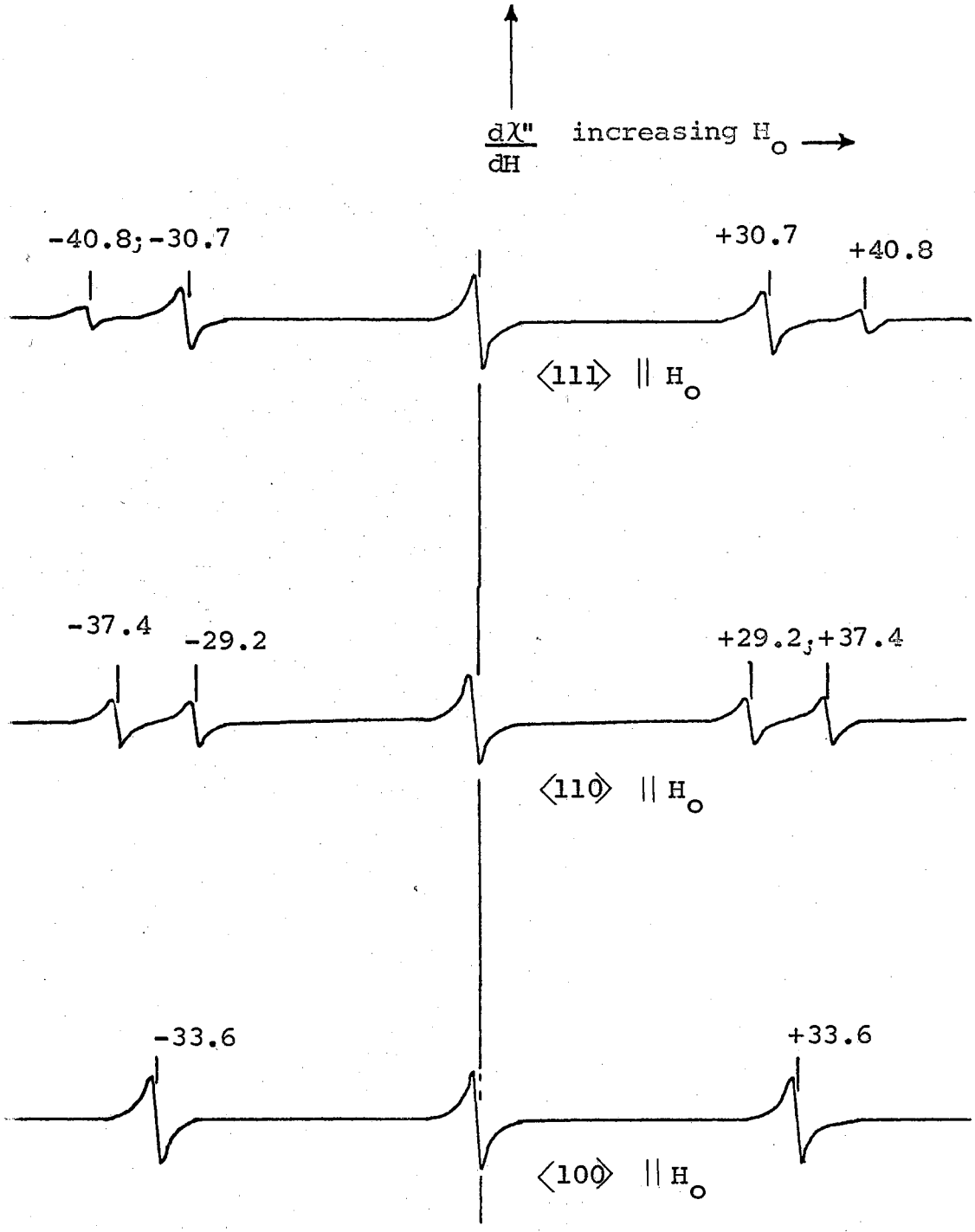

Figure 12. Electron spin resonance of nitrogen in diamond at room temperature.

this study. Since all of the insulating diamonds displayed the nitrogen resonance, only the trace of the complex central structure will be used for comparison purposes. The complete ESR signal for each diamond actually run in this study appears in Appendix A.

Observations

The diamonds investigated were arranged in groups according to their observed color. Diamonds of five different colors were available in the laboratory for use in the experiment. These five colors included clear, yellow, green, brown and blue.

Clear Diamonds

Three clear diamonds were investigated and compared. The diamonds were identified by the letter and number assigned to them in the laboratory diamond inventory and were designated D-76, D-79, and D-3. Diamonds D-76 and D-79 were new diamonds investigated for the first time in this study. Diamond D-3 had been studied previously by King of this laboratory (19) and his data was used for comparison with D-76 and D-79.

All three of the clear diamonds were triangular in shape with flat, parallel, (111) faces. Diamonds D-76

and D-79 were found to be contact twins (macles) (38). There are flat plates with (111) faces and a (111) twin plane parallel to the faces. Because of the twin planes there are three common [110] axes but no common [100] axis. Therefore, the diamonds had to be oriented with common [110] axes parallel to the magnetic field in order to prevent a mixed signal. Diamond D-3 was not reported as a contact twin in the work done by King.

The complex central structure of the three diamonds is shown in Figure 13. No apparent correlation between the clear color of the diamonds and their ESR absorption was found. The signals range in complexity from nineteen on either side of center for D-76 to zero for D-79. Several levels of power and gain were used in the runs on D-79 but no additional signal could be obtained. There was a similarity in the number of peaks between D-3 and D-76 but relative intensities differed greatly. Since orientation studies by many workers have shown the number and relative intensities of complex structures to be greatly dependent upon the orientation, a more extensive study would be necessary before actual similarity between D-3 and D-76 could be established. This investigation was only concerned with obvious correlation within a particular color group and the absence of a signal in

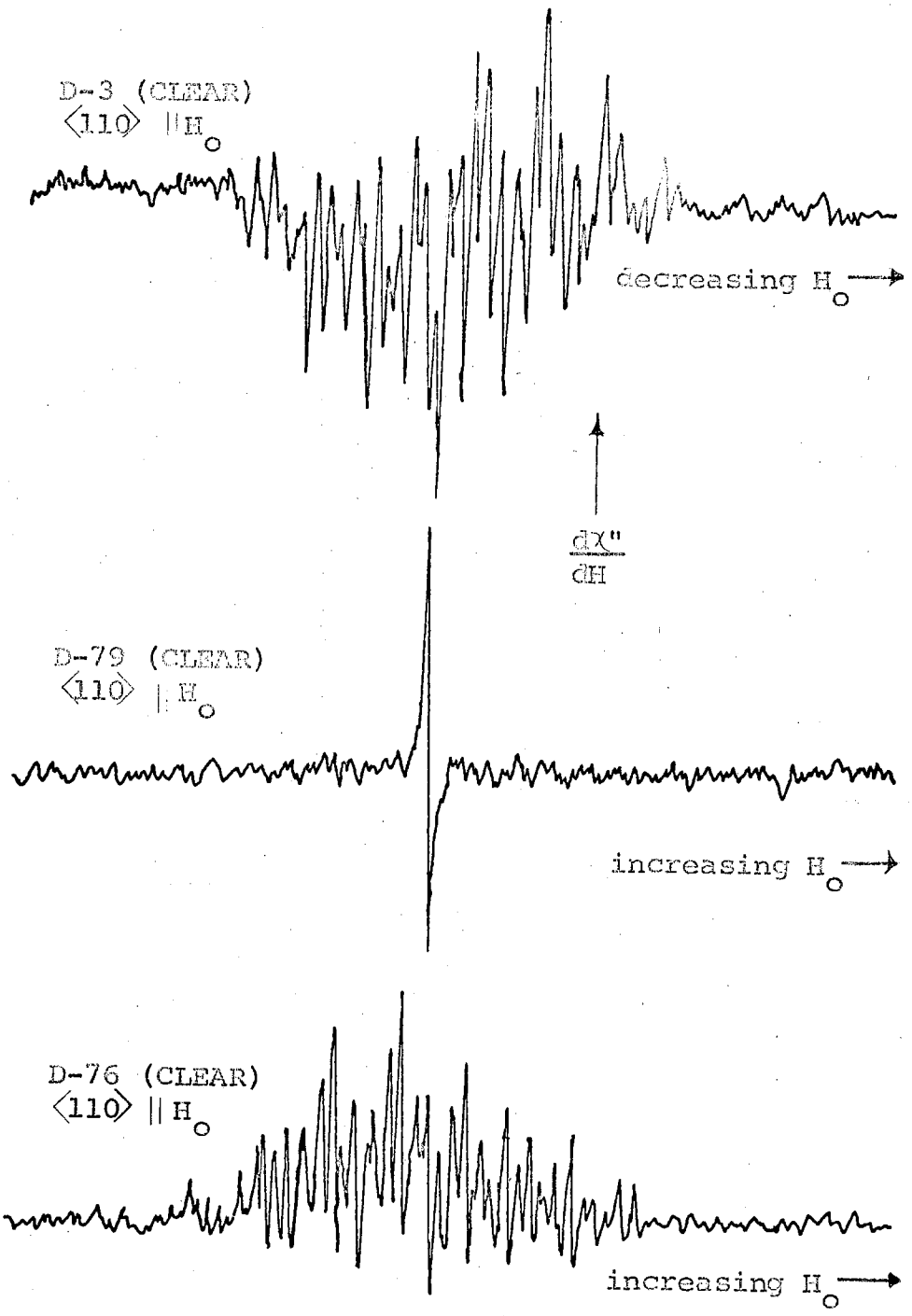

Figure 13. Electron spin resonance of complex center in D-3, D-79, and D-76 with the reference 90° out-of-phase and the power at -17 db.

D-79 was sufficient to rule out correlation within the clear diamond group.

Yellow Diamonds

Data was taken on D-72 and D-73 in the present investigation. The data taken on these two diamonds were compared with data previously taken by King of this laboratory on D-59. All of the yellow diamonds are hexagonal with natural (111) faces forming the flats.

The diamonds in this group displayed similar ESR absorption as shown in Figure 14. The number of peaks in the complex central structure appeared to be the same for all three samples. Comparison of D-59 was difficult because of a poor signal-to-noise ratio and a difference in the direction the magnetic field was scanned. King started at a field strength above resonance and decreased the field. The portion of the signal to the right of center on D-59 had to be compared to the portion to the left of center on D-72 and D-73 because all runs made in the present study were taken using an increasing magnetic field scan. When these difficulties were overcome the signals seemed to show some similarties. There appeared to be fourteen peaks on the low magnetic field side of center and about that many on the high side although some

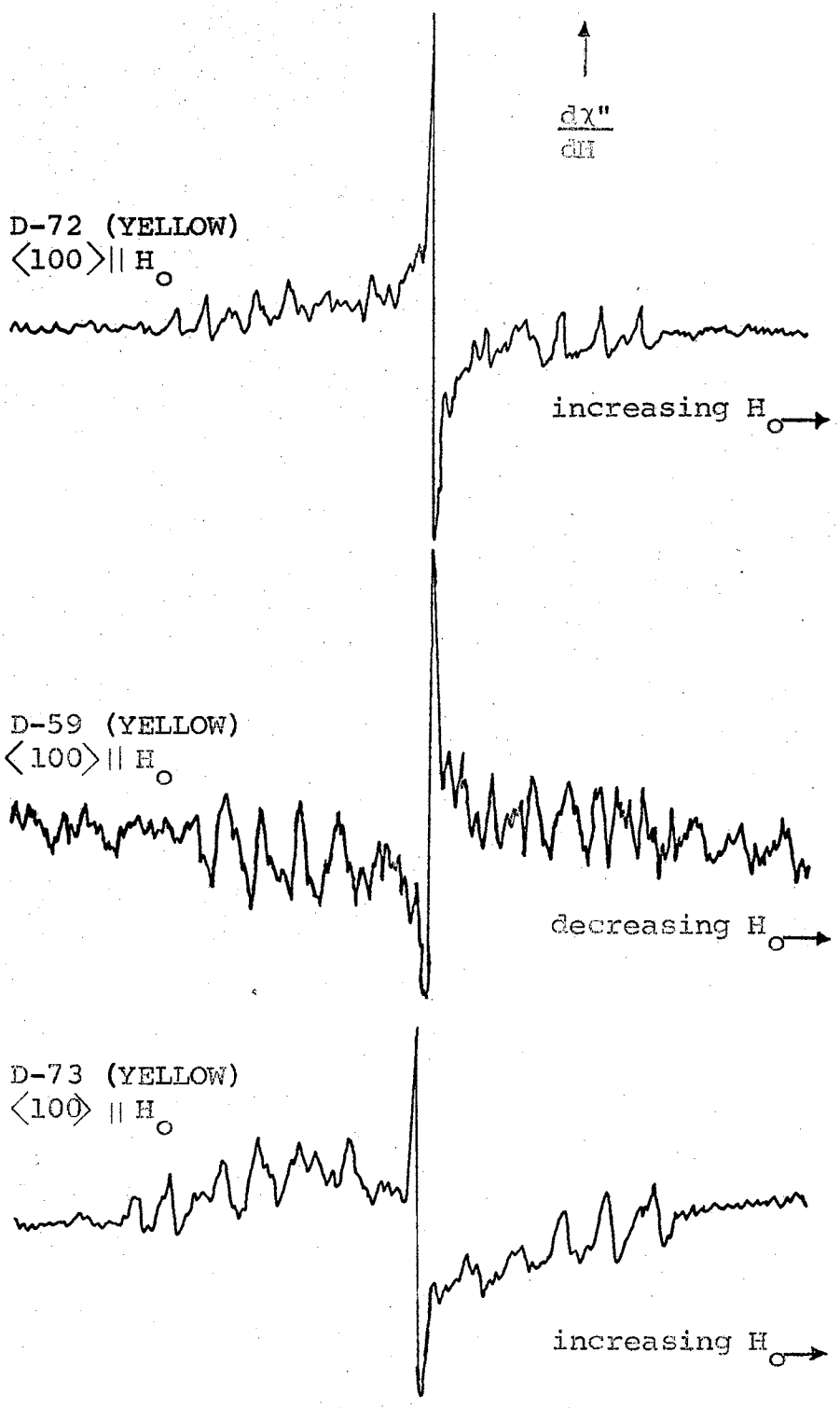

Figure 14. Electron spin resonance of complex center in D-72, D-59, and D-73 with reference 90° out-of-phase and power at -15 db.

were nearly lost in noise. All three had nearly the same signal intensity ratios with the nitrogen signal in each about seven times as strong as the complex structure. Comparison of peak splittings between D-72 and D-59 was very close as were the signal intensities. The signal from D-73 seemed to be spread about 1.5 gauss farther than D-59 or D-72 and the signal intensity ratios showed less than a factor of seven. This difference could have been caused by a small error in orientation. Further study would be necessary, using a large number of yellow diamonds, before conclusive correlation could be established. However, within the scope of this investigation some correlation between the color of yellow diamonds and their ESR absorption was observed.

Green Diamonds

The green diamonds investigated in this study were D-69 and D-74. Their ESR absorption was compared to data previously taken by Bell (26) and Steckelberg (39) of this laboratory on D-57. All three of the green diamonds were approximately oval with no recognizable natural faces. Diamonds D-69 and D-74 were found to be twins and the procedure previously discussed was used to avoid the mixed signals.

The ESR absorption of the three green diamonds with $\langle 110 \rangle \parallel H_o$ is shown in Figure 15. Comparison of the signals shown in Figure 15 did not reveal any apparent correlation. Diamond D-69 had an asymetric signal about the central nitrogen with twenty-one apparent peaks on the low magnetic field side and only sixteen on the high magnetic field side. The substitutional nitrogen signal was not as strong as some of the complex signals and did not stand out. Diamond D-74 appeared to be symetrical about a strong central nitrogen signal with sixteen peaks on each side. The signal intensity of the central nitrogen appeared to be approximately four times as strong as the complex signals. The signal from D-57 was taken by Bell using a decreasing magnetic field scan and the high and low sides of the signal appear reversed compared with D-74 and D-69. Diamond D-57 appears to be symetrical about a central nitrogen peak with eight peaks on each side. The central nitrogen signal is only about twice as strong as the complex signals.

An additional comparison was made between D-69 and D-57 with $\langle 113 \rangle \parallel H_o$ as shown in Figure 16. Diamond D-69 appeared to be symetrical about a central nitrogen peak when oriented with the $\langle 113 \rangle \parallel H_o$ and had fifteen peaks on each side for the in-phase run shown in Figure 16.

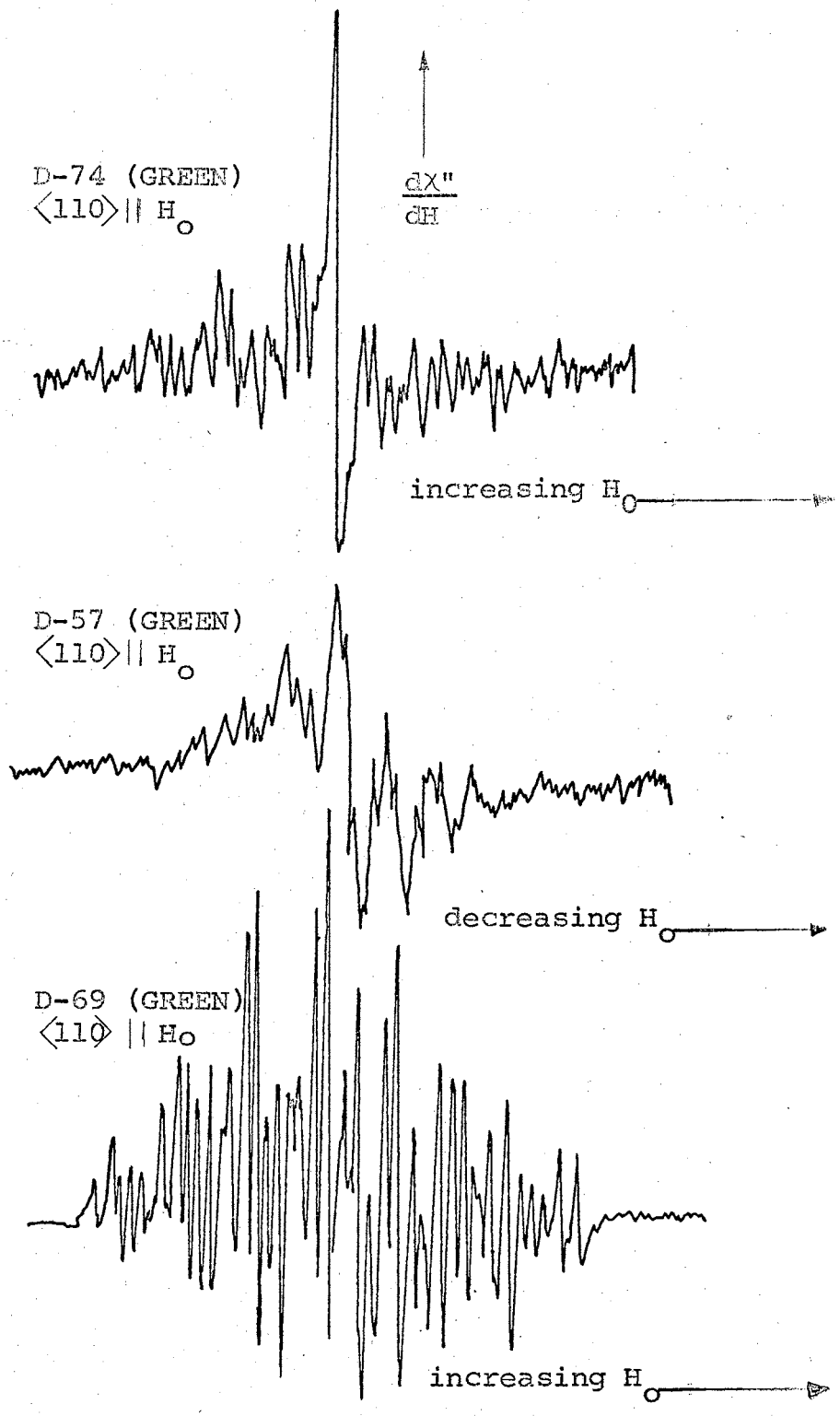

Figure 15. Electron spin resonance of complex center in D-74, D-57, and D-69 with reference 90° out-of-phase and power at -15 db.

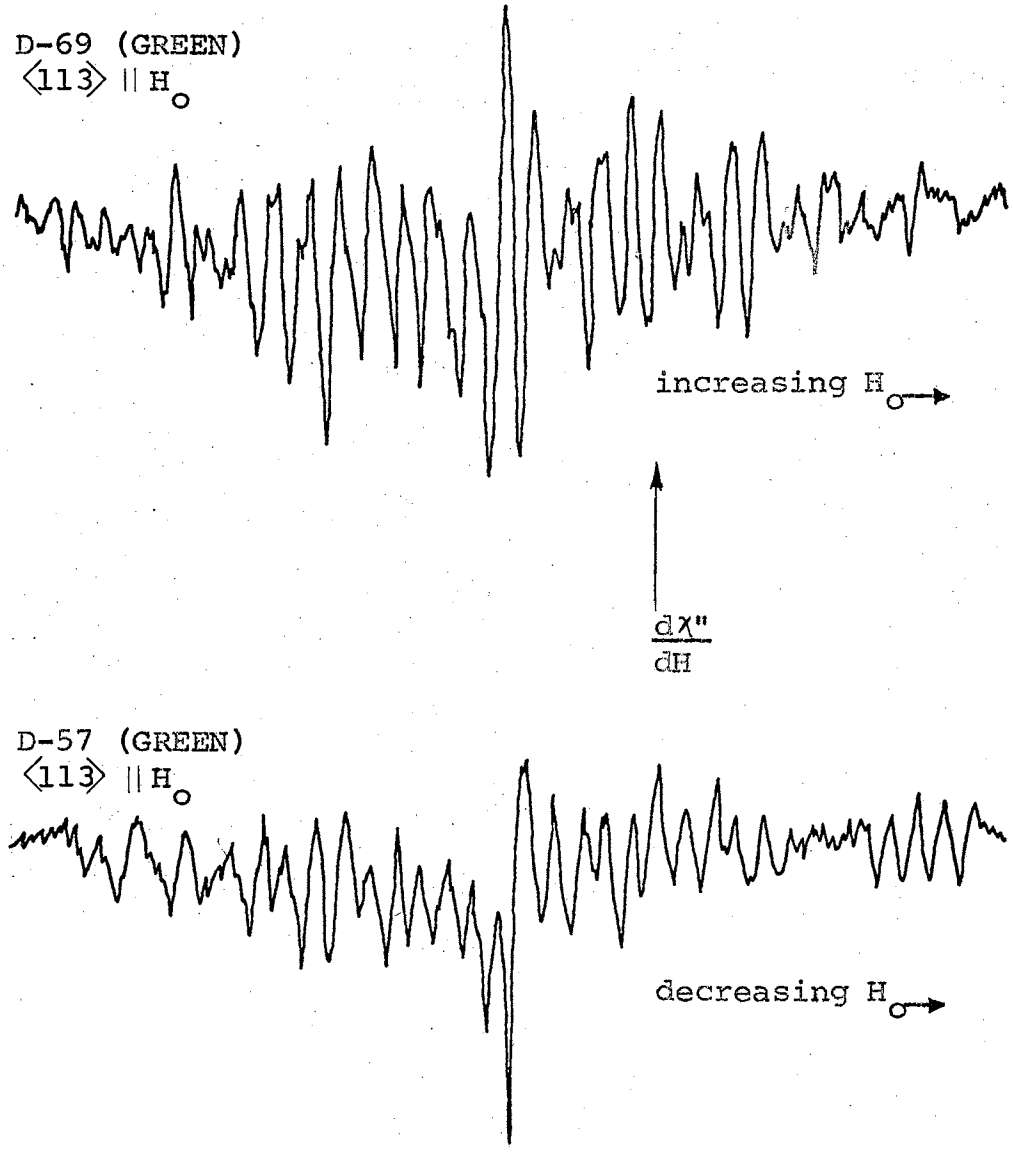

Figure 16. Electron spin resonance of complex center in D-69, and D-57 with reference phase in-phase, power at -40 db, and slow scan rate.

Diamond D-57 did not appear to be symetrical about the central nitrogen signal when oriented in this direction and had only twelve peaks on the low magnetic field side while showing at least fourteen on the high magnetic field side.

There appeared to be very little apparent correlation between the color of green diamonds and their ESR absorption signal.

Brown Diamonds

No brown diamonds were available for direct use in this investigation. Therefore, a comparison was made using data taken by King and Steckelberg on D-61 and D-60. Steckelberg reported on D-60 and D-61 as brown diamonds with smooth flat surfaces that were (110) planes (39). Figure 17 shows comparisons of two different orientations for these diamonds. Both diamonds had strong nitrogen central peaks with very little complex structure showing. Diamond D-61 displayed some complex structure but the complex signal displayed by D-60 was too weak to allow accurate comparison. On the basis of the previous work done on D-60 and D-61, there seemed to be some similarity between the absorption of the two samples. However, the signal intensity ratios were not

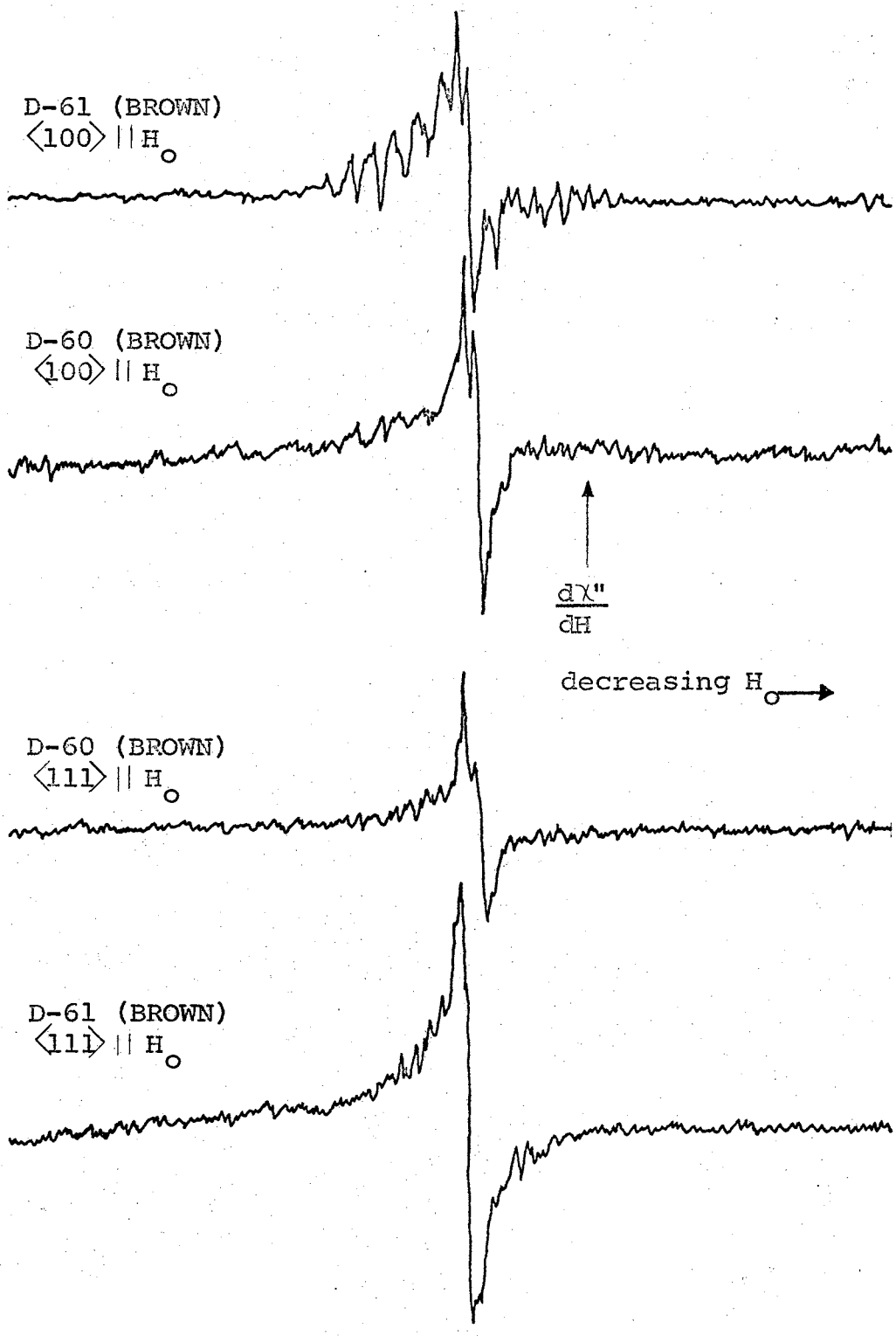

Figure 17. Electron spin resonance of complex center in D-60 and D-61 with reference in-phase and power at -30 db.

the same for the samples and D-60 displayed no apparent peaks comparable to those in D-61.

Blue Diamonds

No blue diamonds were available for direct use in this investigation. Therefore, the data used for comparison was obtained by Bell in a previous study (26). Bell used semiconducting diamonds DS-5 and DS-3 which were steel-blue in color and different in shape due to cutting and polishing. Diamond DS-3 was reported by Bell to be a gem stone with a marquise cut while DS-5 was a large semiconductor with two parallel (111) faces.

The ESR absorptions for DS-5 at 4.2^{o}K and DS-3 at room temperature are shown in Figure 18. Both diamonds show only a broad absorption signal near g = 2 and no nitrogen signals. Diamond DS-3 has a central peak which tapers off for approximately ten gauss to both sides before reaching zero. Diamond DS-5 at 4.2^{o}K displayed a central peak with a half-width of 5.5 gauss.

There seemed to be a direct correlation between the color of blue diamonds and their ESR absorption. Work done by other workers in this laboratory has indicated that most semiconducting diamonds are blue and that they all seem to display one characteristic, broad, ESR

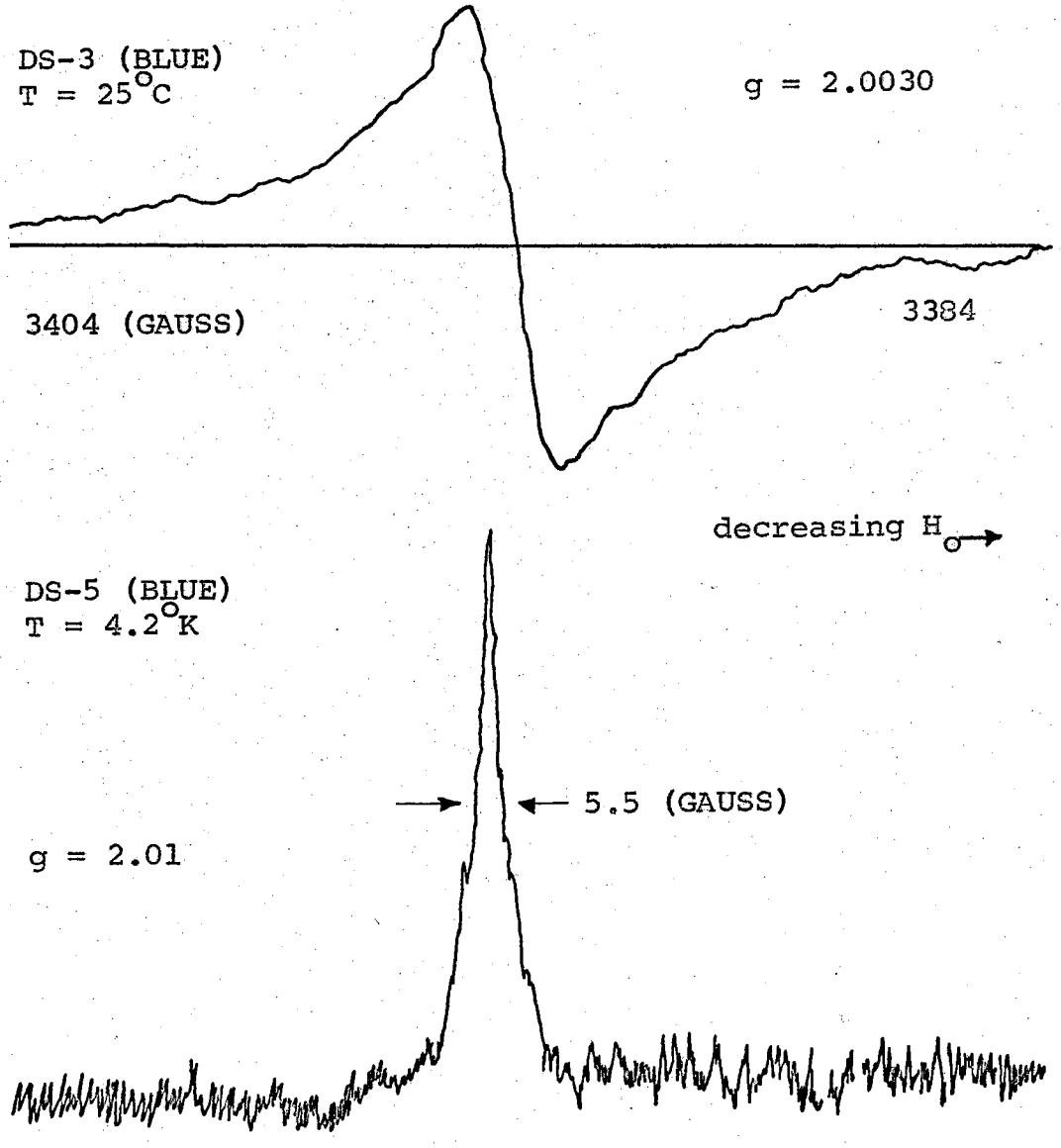

Figure 18. Electron spin resonance in DS-3 and DS-5.

absorption signal.

Discussion and Summary

A correlation of color and ESR absorption in diamond was investigated for five differently colored groups of diamonds. The only color groups to display apparent correlation were the group of yellow diamonds and the group of blue semiconducting diamonds. Every blue diamond displayed a broad ESR absorption with no nitrogen signal. The apparent correlation in the yellow group should be investigated further if a large number of yellow diamonds is available. It was noted however, that diamonds within the same color group displayed similar crystal growth habits.

A SELECTED BIBLIOGRAPHY

(1) G. W. Ludwig and H. H. Woodbury, "Electron Spin Resonance in Semiconductors," Solid State Physics 13, 223 (1962).

(2) D. J. E. Ingram, Free Radicals as Studied by Electron Spin Resonance, (Butterworths Scientific Publications, London, 1958).

(3) J. Uebersfeld, "Spectrometre pour Resonance Paramagnetique," Ann. phys. 1, 395 (1956).

(4) B. W. Shore and D. H. Menzel, Principles of Atomic Spectra, (John Wiley and Sons, Inc., New York, 1968).

(5) R. Robertson, J. J. Fox, and A. E. Martin, "Two Types of Diamond," Phil. Trans. Roy. Soc. (London) A232, 463 (1934).

(6) G. B. B. M. Sutherland, D. E. Blackwell, and W. G. Simeral, "The Problem of the Two Types of Diamond," Nature 174, 901 (1954).

(7) C. D. Clark, R. W. Ditchburn, and H. B. Dyer, "The Absorption Spectra of Natural and Irradiated Diamonds," Proc. Roy. Soc. (London) A234, 363 (1956).

(8) J. F. H. Custers, "Unusual Phosphorescence of a Diamond," Physics 18, 489 (1952).

(9) J. F. H. Custers, "Semiconductivity of Type IIb Diamonds," Nature 176, 173 (1955).

(10) J. F. H. Custers, "Type IIb Diamond," Physics 20, 183 (1954).

(11) H. J. Stein, M. D. Bell, and W. J. Leivo, "Optical Studies on Semiconducting Diamond," Bull. Am. Phys. Soc. 1, 127 (1956).

(12) H. J. Stein, "Determination of Energy Levels in Semiconducting Diamond by Transmission Method," (M. S. thesis, Oklahoma State University, 1960).

(13) W. Kaiser and W. L. Bond, "Nitrogen, a Major Impurity in Common Type I Diamond," Phys. Rev. 115, 857 (1959).

(14) E. C. Lightowlers and P. J. Dean, "Measurement of Nitrogen Concentration in Diamond by Photon Analysis and Optical Absorption," Diamond Research (1964).

(15) W. V. Smith, P. P. Sorokin, I. L. Gelles, and G. J. Lasher, "Electron Spin Resonance of Nitrogen Donors in Diamond," Phys. Rev. 115, 1546 (1959).

(16) W. V. Smith, I. L. Gelles, and P. P. Sorokin, "Electron Spin Resonance of Acceptor States in Diamond," Phys. Rev. Letter 2, 39 (1959).

(17) M. D. Bell and W. J. Leivo, "Electron Spin Resonance in Semiconducting Diamond," Bull. Am. Phys. Soc. 6, 142 (1961).

(18) G. K. Walters and T. L. Estle, "Paramagnetic Resonance of Defects Introduced Near the Surface of Solids by Mechanical Damage," J. Appl. Phys. 32, 1854 (1961).

(19) J. P. King, "Effects of Light on the Electron Spin Resonance of Diamond," (Ph. D. thesis, Oklahoma State University, 1966).

(20) R. Berman, Physical Properties of Diamond, (Clarendon Press, Oxford, 1965).

(21) T. L. Squires, An Introduction to Electron Spin Resonance, (Academic Press, New York, 1964).

(22) J. I. Rabi, N. F. Ramsey, and J. Schwinger, "Use of Rotating Coordinates in Magnetic Resonance Problems," Rev. Mod. Phys. 26, 167 (1954).

(23) F. Bloch, "Nuclear Induction," Phys. Rev. 70, 460 (1946).

(24) A. Abragam, Principles of Nuclear Magnetism, (Oxford University Press, London, 1961).

(25) A. C. Melissinos, Experiments in Modern Physics, (Academic Press, New York, 1966).

(26) M. D. Bell, "Electron Spin Resonance in Diamond," (Ph. D. thesis, Oklahoma State University, 1964).

(27) J. W. M. DuMond and E. R. Cohen, Handbook of Physics, (McGraw-Hill Co., New York, 1962).

(28) J. P. Gorden, "Variable Coupling Reflection Cavity for Microwave Spectroscopy," Rev. of Sci. Instr. 32, 658 (1961).

(29) R. Ager, T. Cole, and J. Lambe, "Coupling Scheme for Microwave Cavities," Rev. Sci. Instr. 32, 658 (1961).

(30) F. A. Faulkner, "Improved Circuit for an Electron Spin Resonance Spectrometer," J. Sci. Instr. 39, 135 (1962).

(31) B. Lax and K. J. Button, Microwave Ferrites and Ferrimagnetics ,(McGraw-Hill Co., New York, 1962).

(32) A. M. Portis, "Electronic Structure of F Centers: Saturation of the Electron Spin Resonance," Phys. Rev. 91, 1071 (1953).

(33) C. G. Montgomery, Techniques of Microwave Measurements, MIT Radiation Lab. Series, Vol. 11, (Mc-Graw-Hill, New York, 1947).

(34) R. V. Pound, "Frequency Stablization of Microwave Oscillators," Proc. of IRE 34, 1405 (1947).

(35) M. W. P. Stranberg, M. Tinkham, I. H. Solt Jr., and C. F. Davis, "Recording Magnetic-Resonance Spectrometer," Rev. Sci. Instr. 27, 596 (1956).

(36) F. P. Zaffarano and W. C. Galloway, "Notes on the Pound Microwave Frequency Stabilizer," Technical Report #31, Research Laboratory of Electronics, MIT (1947).

(37) W. Low, "Paramagnetic Resonance in Solids," Solid State Phys. Supplement 2, 1 (1960).

(38) T. Evans and C. Phaal, "Imperfections in Type I and Type II Diamonds," Proc. Roy. Soc. (London) A270, 538 (1962).

(39) W. C. Steckelberg, "Electron Spin Resonance Symmetry Study of Type I Diamond," (unpub. M. S. thesis, Oklahoma State University, 1967).

(40) C. Kittel, Introduction to Solid State Physics, (John Wiley and Sons, Inc., New York, 1959), p. 65.

(41) R. V. Pound, "Electronic Frequency Stabilization of Microwave Oscillators," Rev. Sci. Instr. 17, 49 (1946).

(42) C. P. Slichter, Principles of Magnetic Resonance, (Harper and Row, New York, 1963).

(43) P. A. M. Dirac, Principles of Quantum Mechanics, (Oxford at the Clarendon Press, Oxford, 1959).

(44) G. E. Pake, "Fundamentals of Nuclear Magnetic Resonance Absorption," Am. J. of Phys. 18, 438 (1950).

(45) G. E. Pake, Paramagnetic Resonance,(W. A. Benjamin, New York, 1962).

(46) J. C. Slater, Microwave Electronics, (D. Van Nostrand Co., New York, 1950).

(47) Anon., "Nitrogen in Diamond Governs Their Shape and Color," S. Afc. Engng. J. 5, 2973 (1956).

(48) W. Gordy, W. V. Smith, and R. F. Trambarulo, Microwave Spectroscopy, (Dover Publications, Inc., New York, 1953).

(49) W. C. Lochart and R. C. Jones, " EPR Spectrometers: Operating Fundamentals," NMR and EPR Spectroscopy, (Pergamon Press, New York, 1960).

(50) R. H. Sands, "EPR Spectroscopy," NMR and EPR Spectroscopy, (Pergamon Press, New York, 1960).

(51) C. P. Poole, Electron Spin Resonance, (Interscience Publishers, New York, 1967).

(52) J. P. McKelvey, Solid State and Semiconductor Physics, (Harper and Row, Publishers, New York, 1966).

(53) C. H. Blanchard, C. R. Burnett, R. G. Stoner, and R. L. Weber, Introduction to Modern Physics, (Prentice-Hall, Inc., New Jersey, 1956) p. 181.

(54) V. Rojansky, Introductory Quantum Mechanics, (Prentice-Hall, Inc., New Jersey, 1938) p. 477.

APPENDIX A

SAMPLES OF ACTUAL RECORDER GRAPHS USED IN THE STUDY

The actual recorder graphs could not be photographed directly because of the color of ink used in the recorder pen. Therefore, it was necessary to trace the actual graphic representations as accurately as possible and use these for comparison purposes in the body of the thesis. Since it was desirable to include actual copies of the recorder graphs showing all noise and exact signal ratios, these were Xeroxed individually and appear on the following pages. The complete ESR signal for each diamond actually run in this study is shown for the desired orientation. Copies of recorder graphs of the complex centers are also shown for both normal and slow scan rates. Other important information concerning each graph is indicated on the figure. This information indicates the gain of the amplifier, the amplitude of the modulation signal, the power level being feed to the sample cavity, and the phase of the reference signal for each of the graphs. The graphs appear in the order in which the diamonds are discussed in the study.

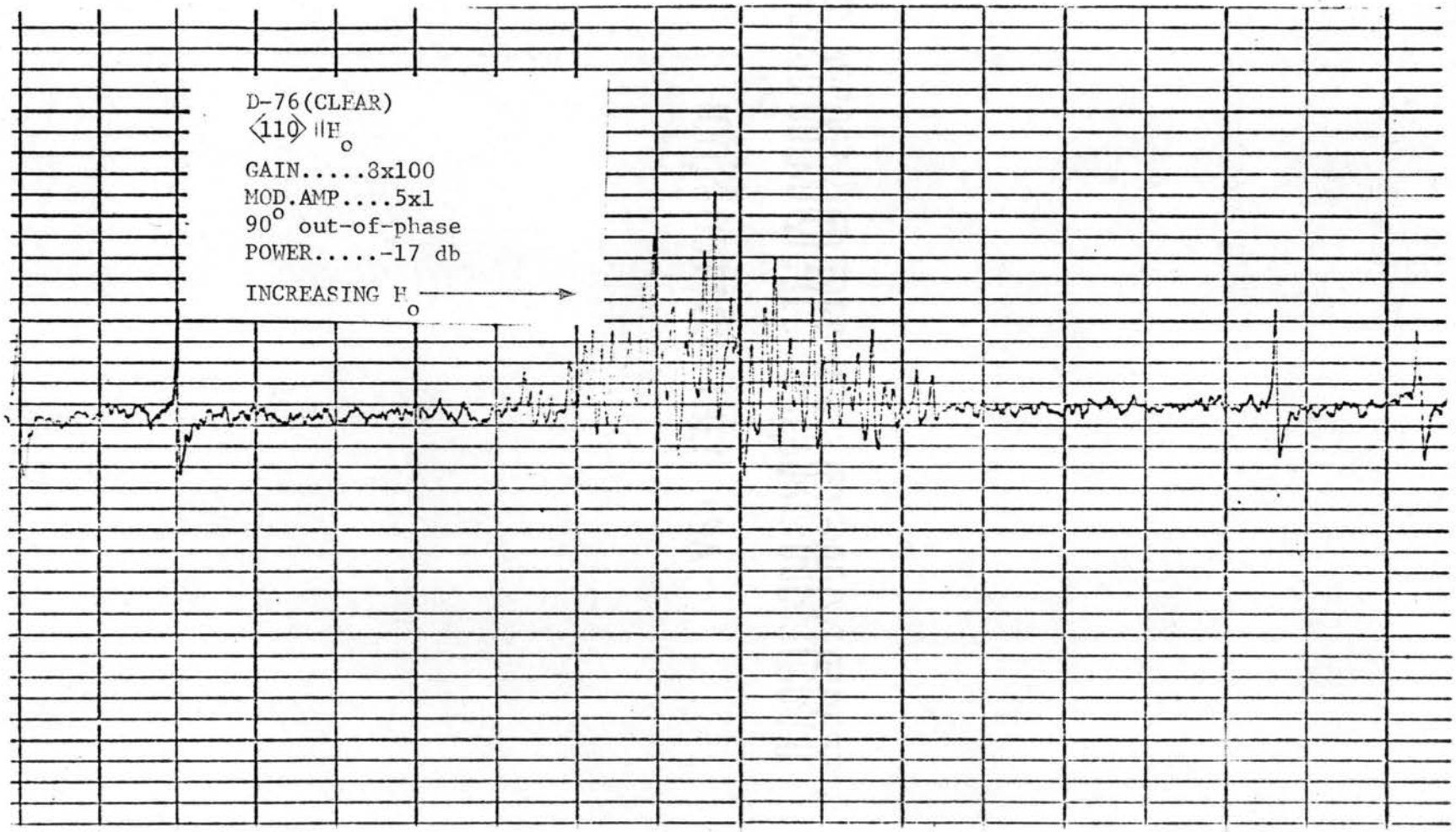

Figure 19. Electron spin resonance in D-76 (CLEAR).

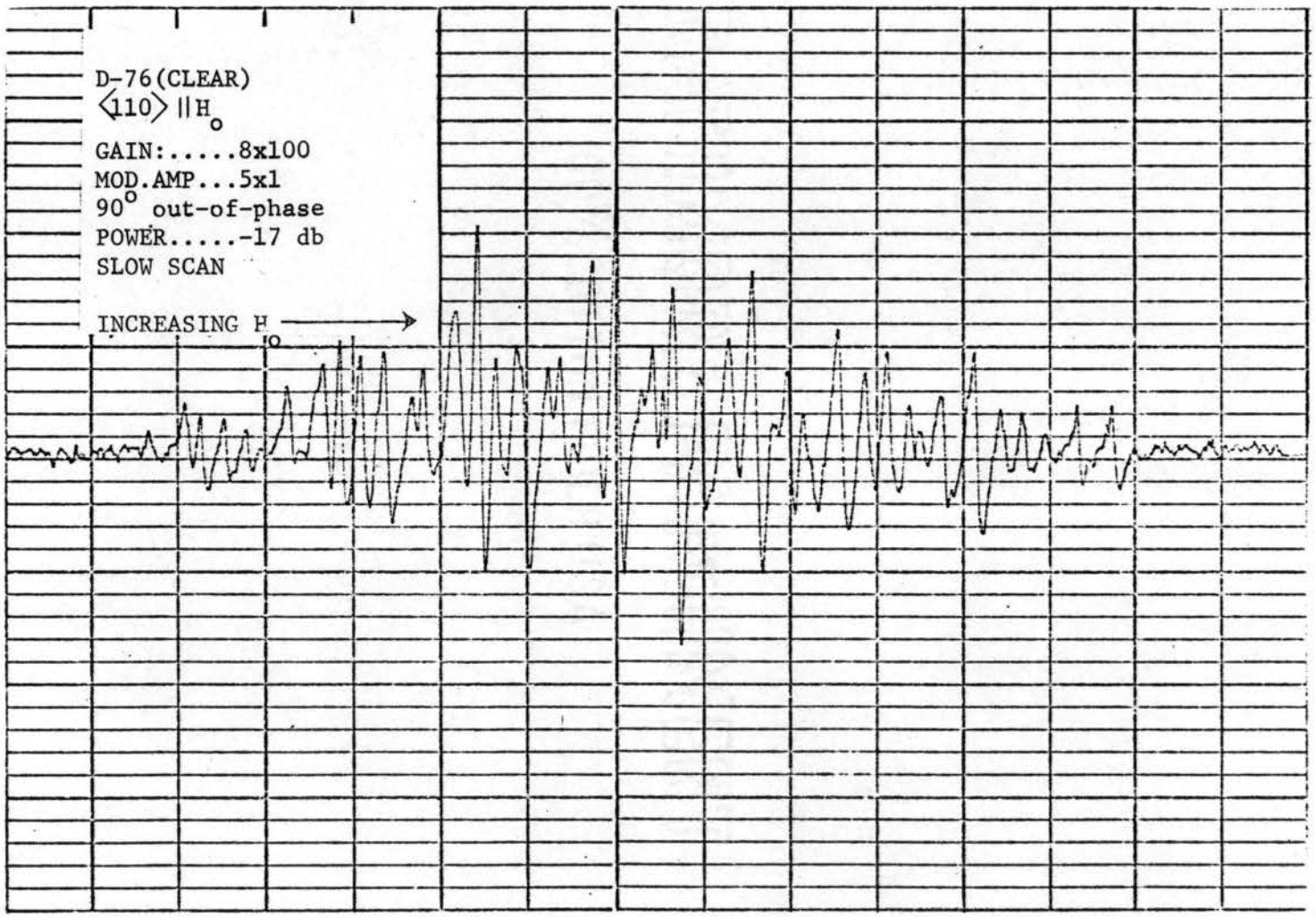

Figure 20. Electron spin resonance of complex center in D-76(CLEAR).

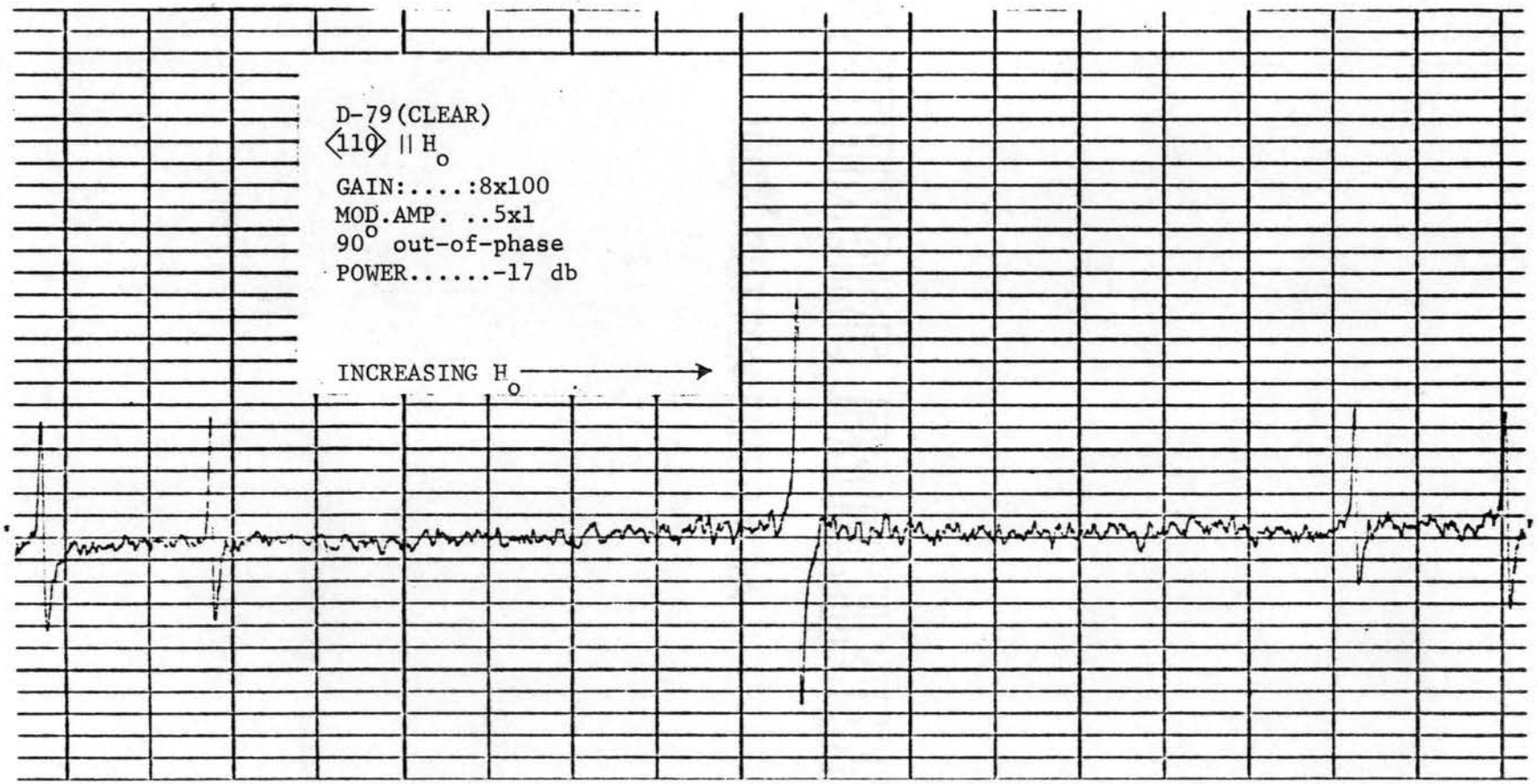

Figure 21. Electron spin resonance in D-79(CLEAR).

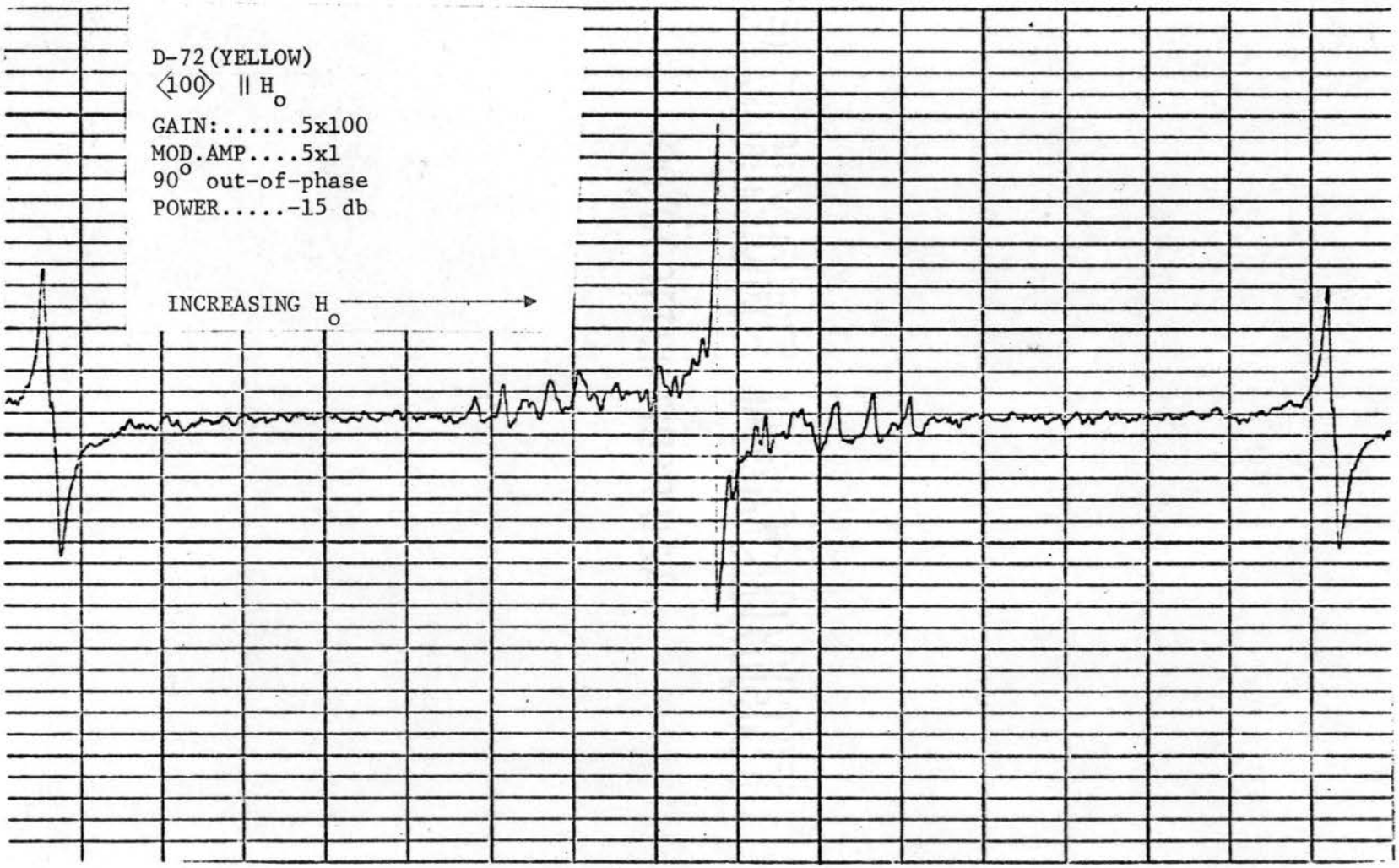

Figure 22. Electron spin resonance in D-72(YELLOW).

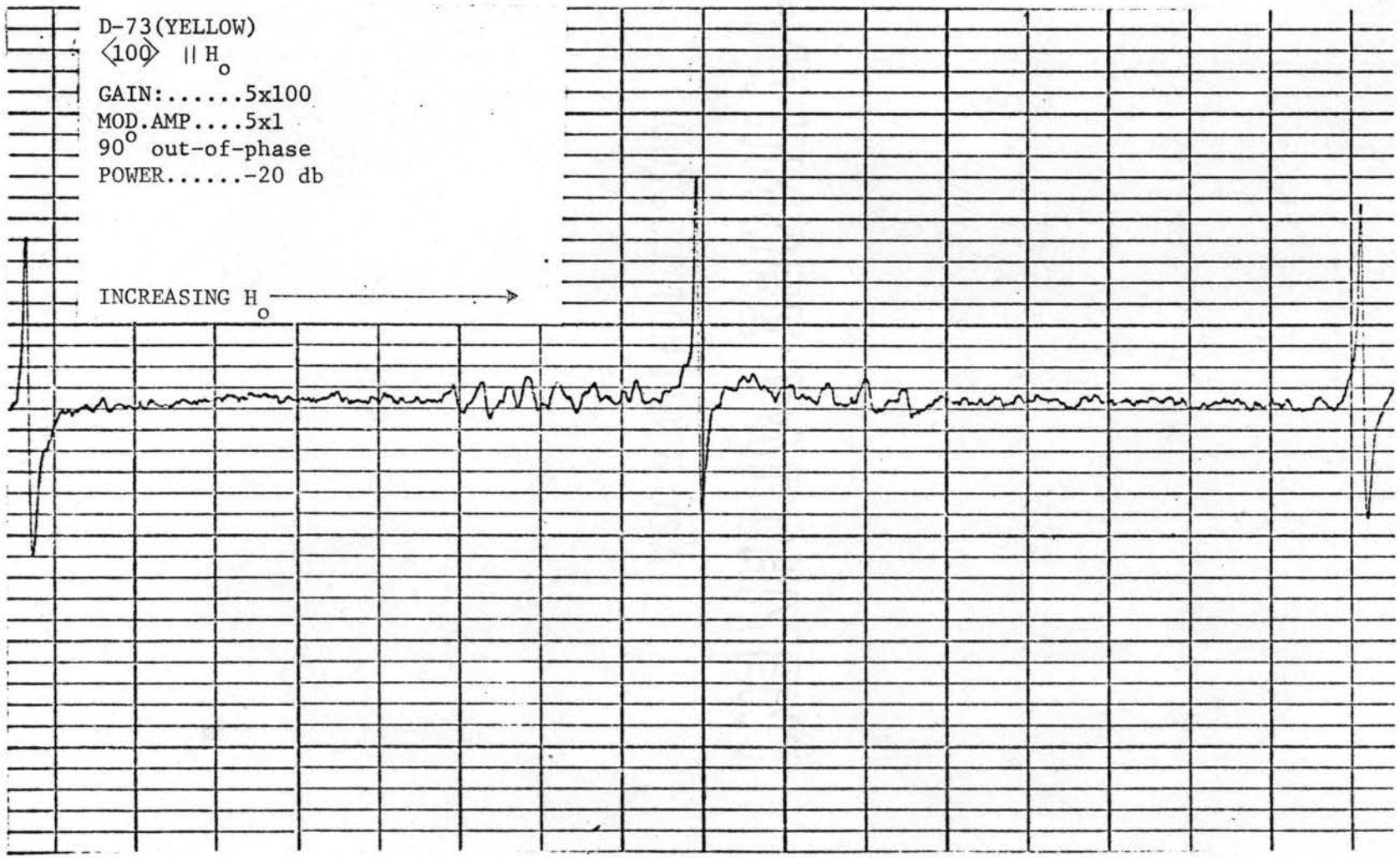

Figure 23. Electron spin resonance in D-73(YELLOW).

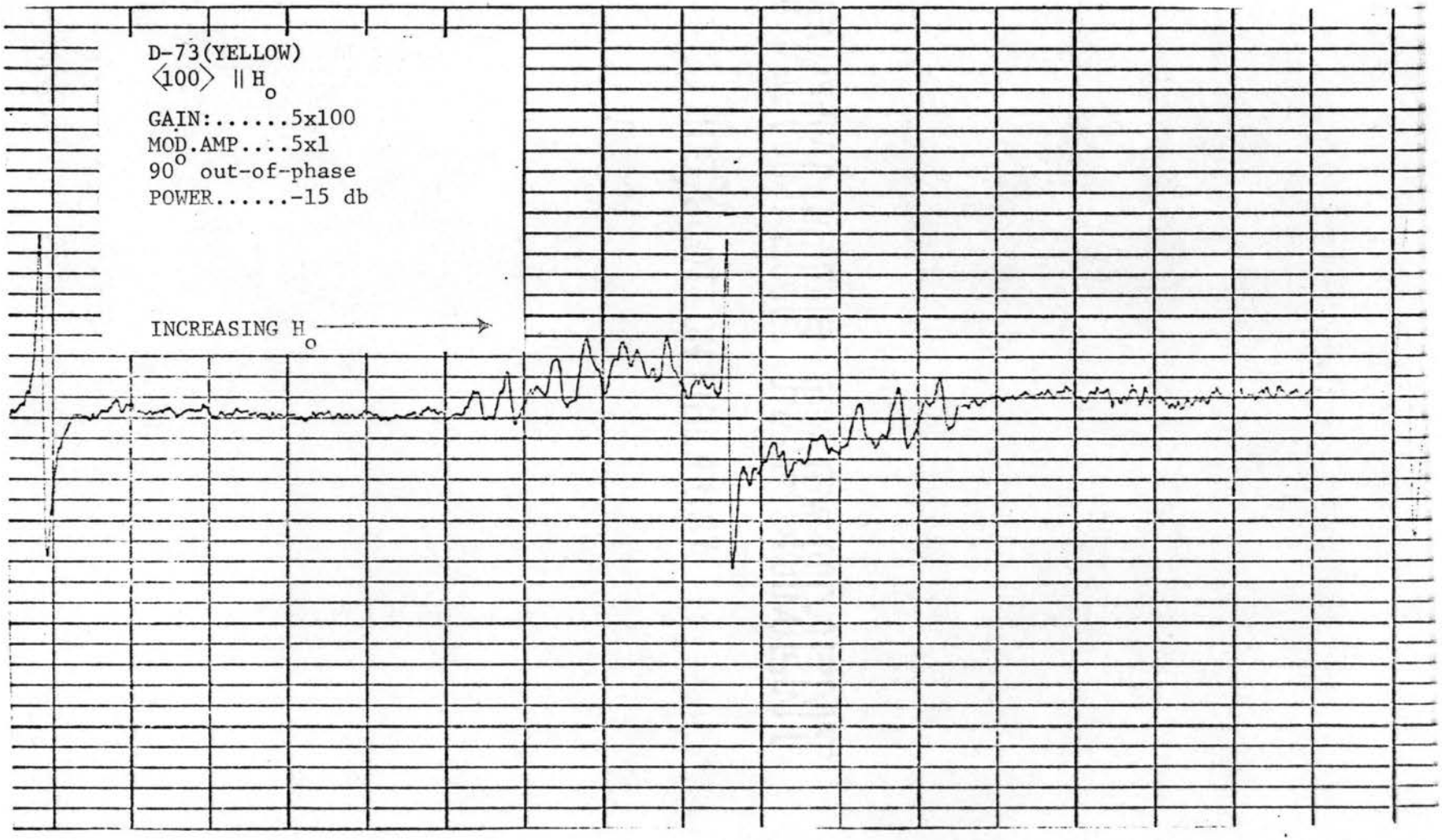

Figure 24. Electron spin resonance in D-73(YELLOW).

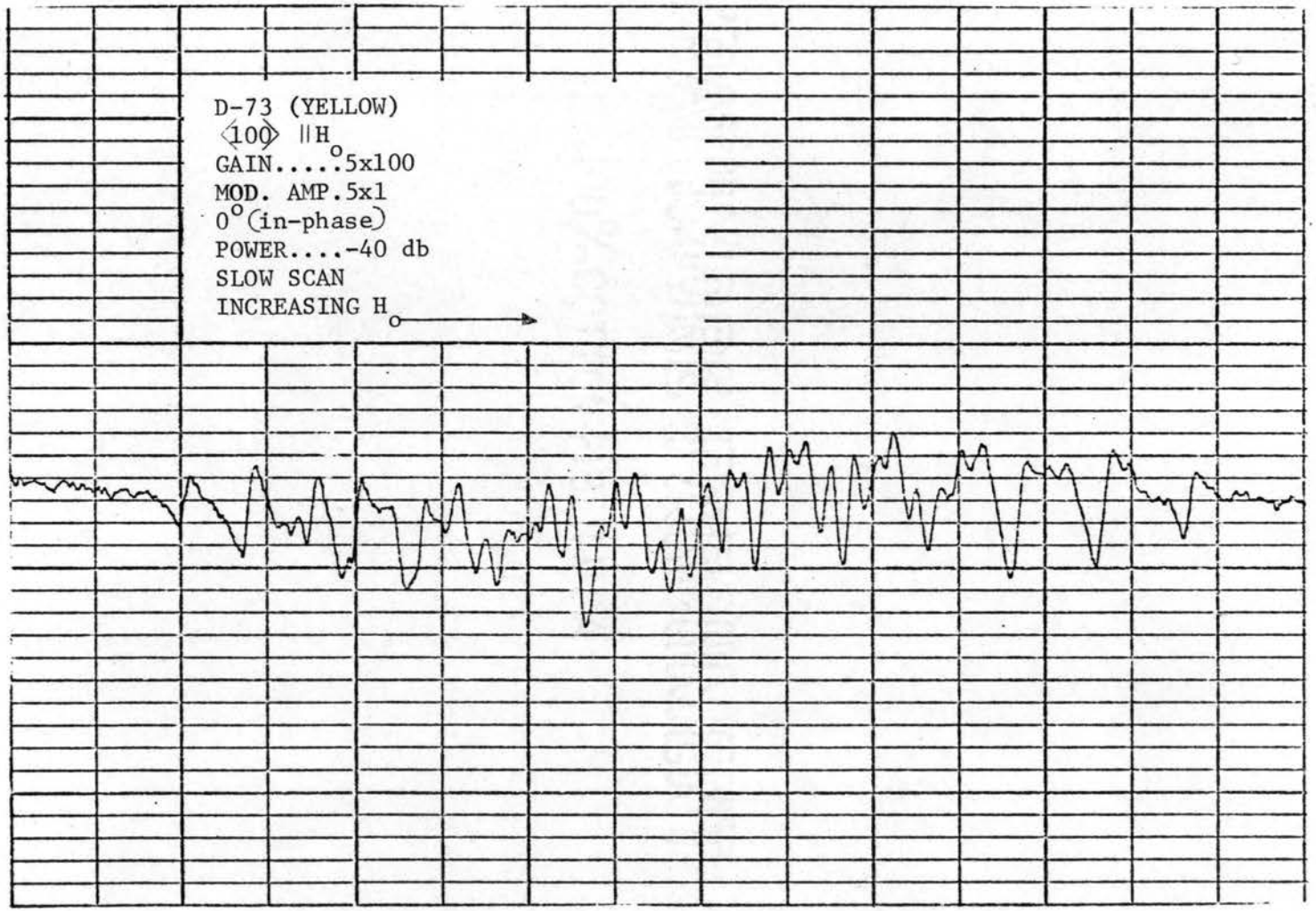

Figure 25. Electron spin resonance of complex center in D-73 (YELLOW).

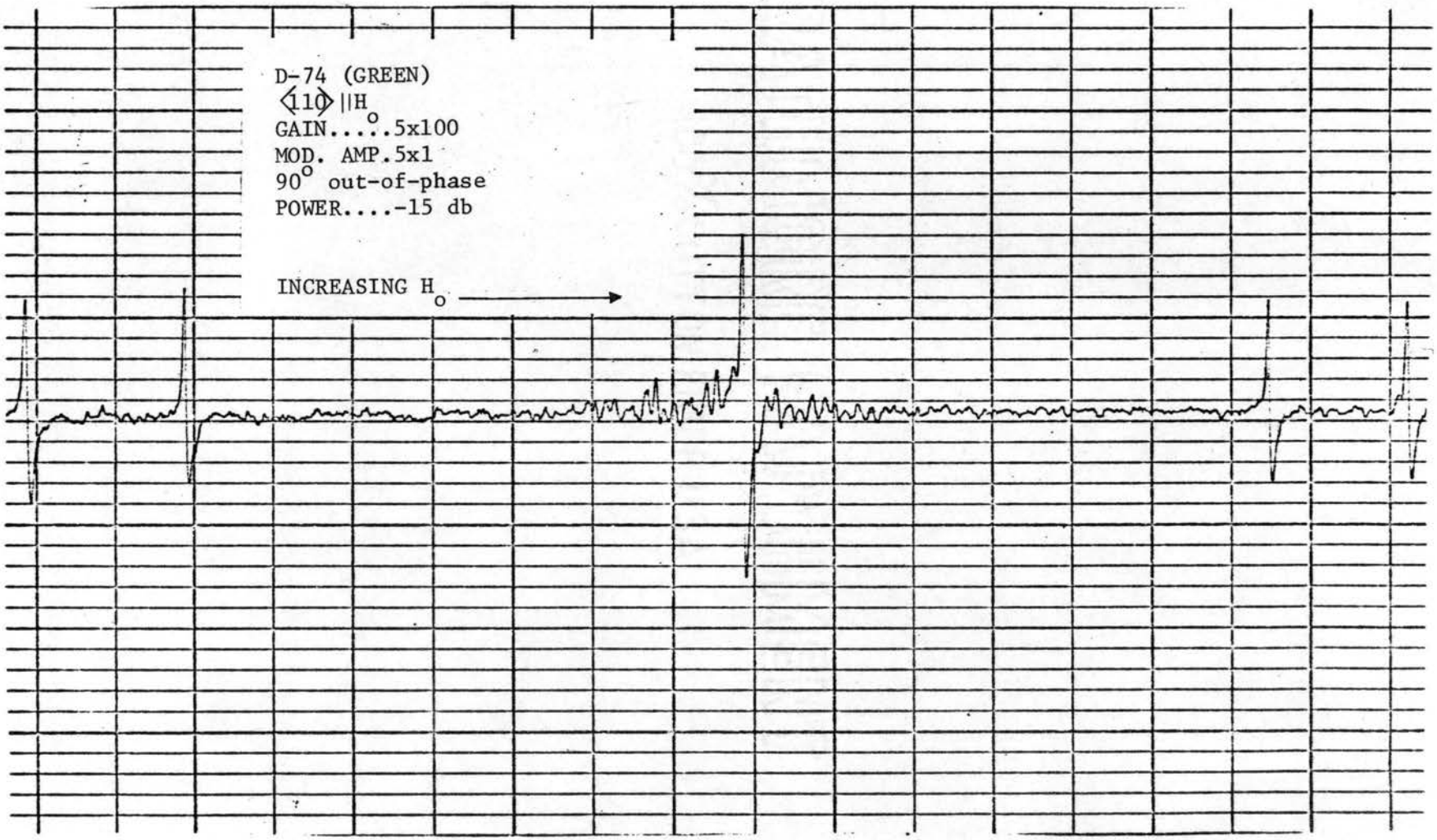

Figure 26. Electron spin resonance in D-74 (GREEN).

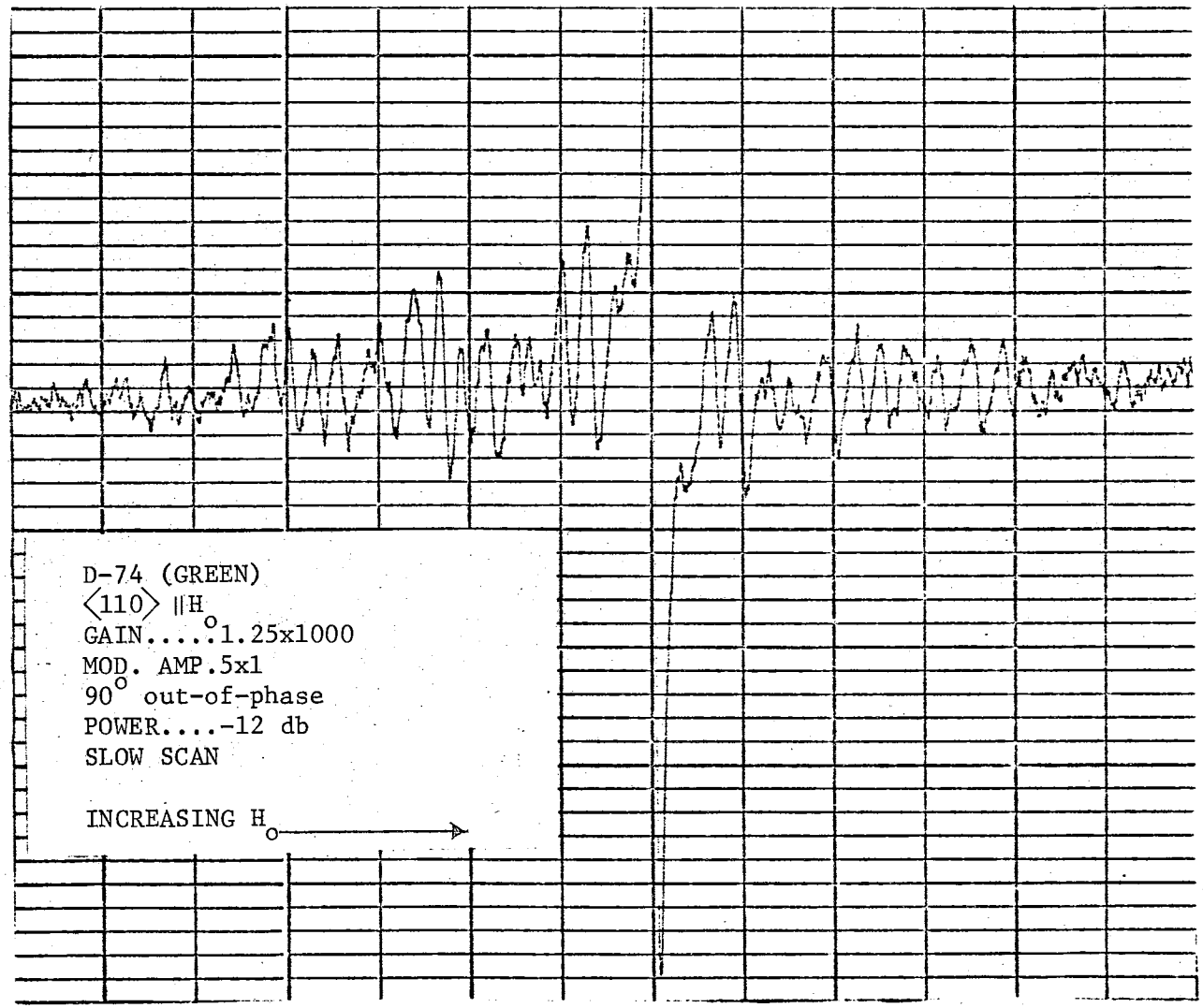

Figure 27. Electron spin resonance of complex centers in D-74 (GREEN).

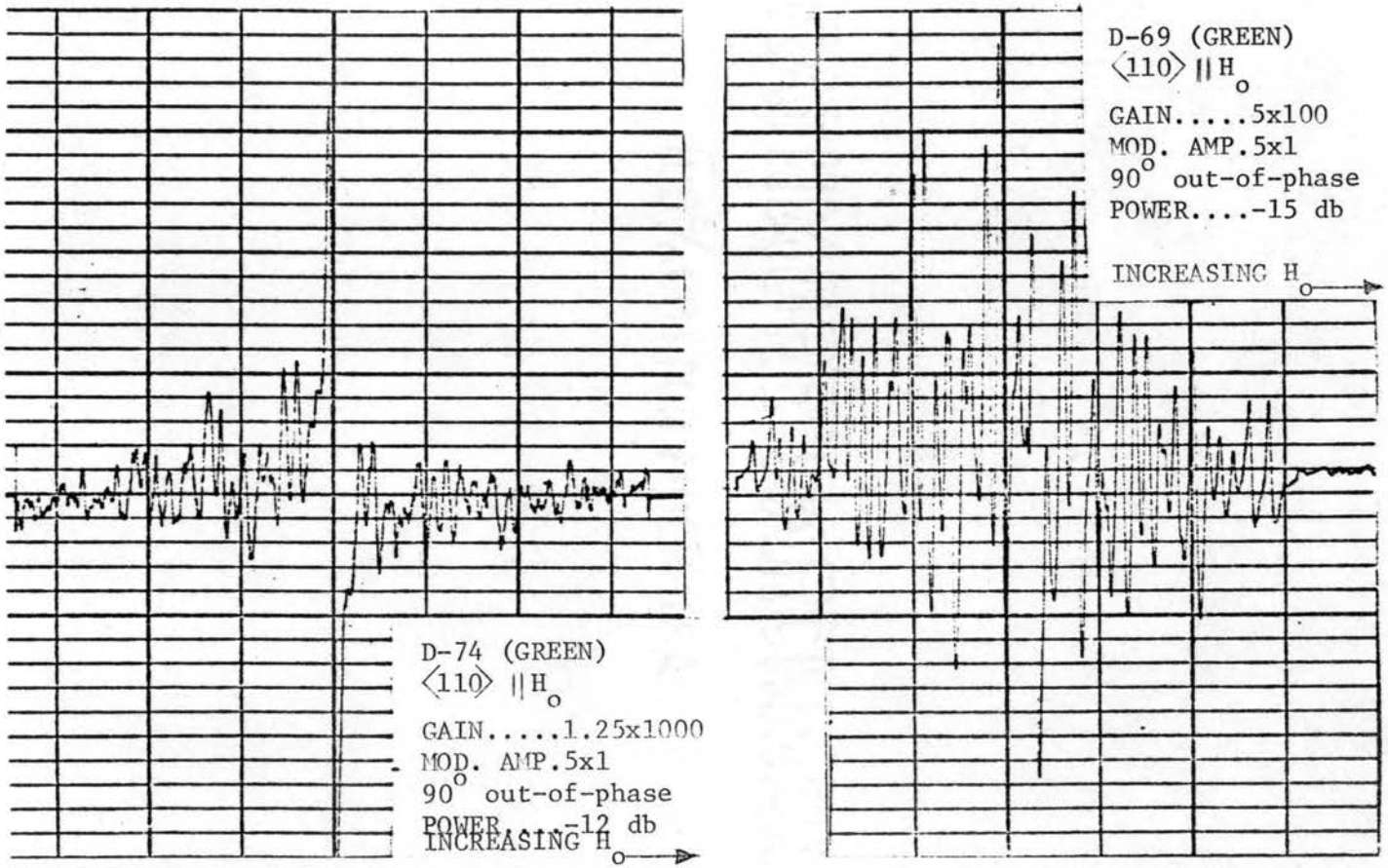

Figure 28. Electron spin resonance of complex center in D-74 and D-69 (GREEN).

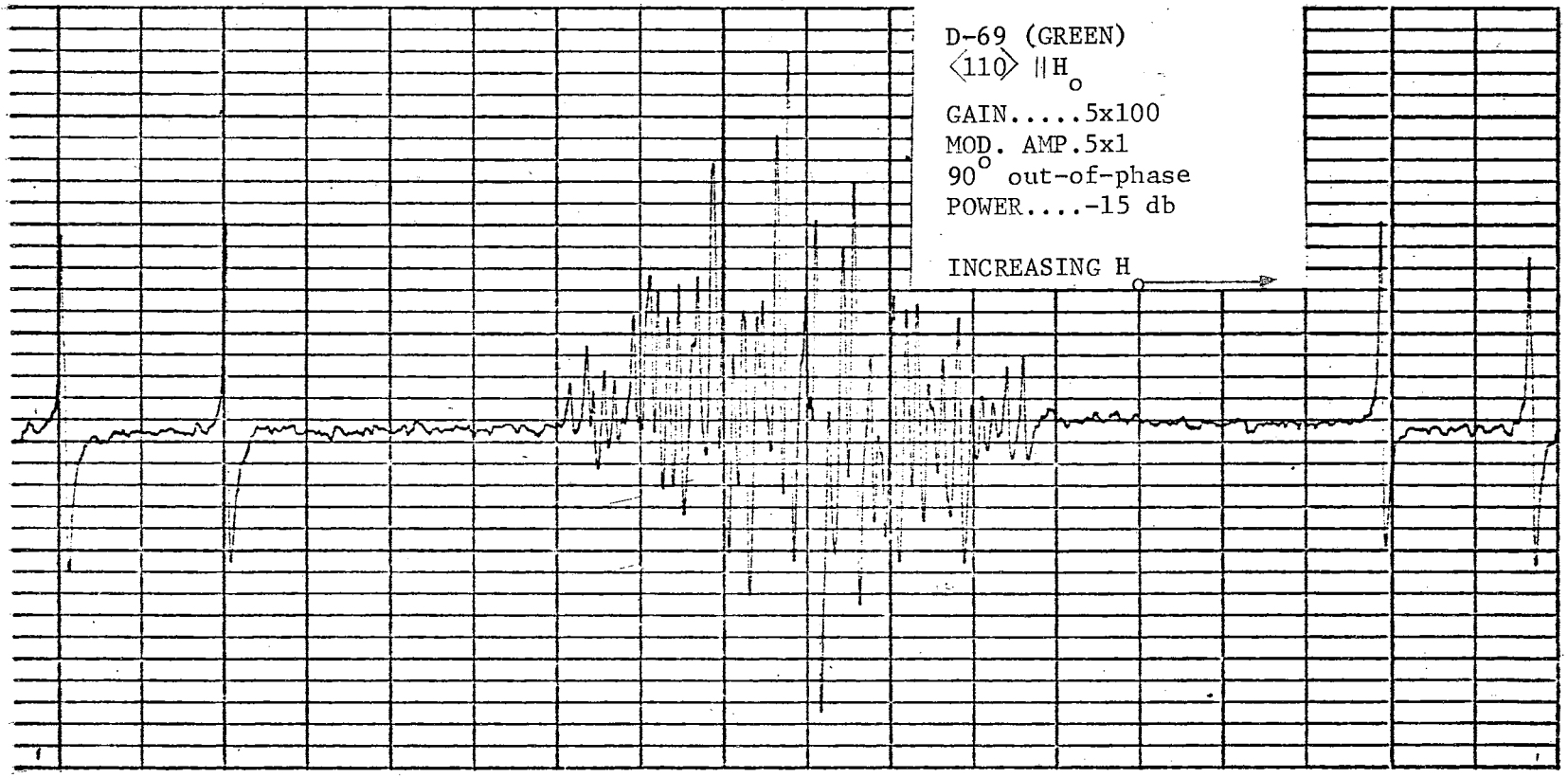

Figure 29. Electron spin resonance in D-69 (GREEN).

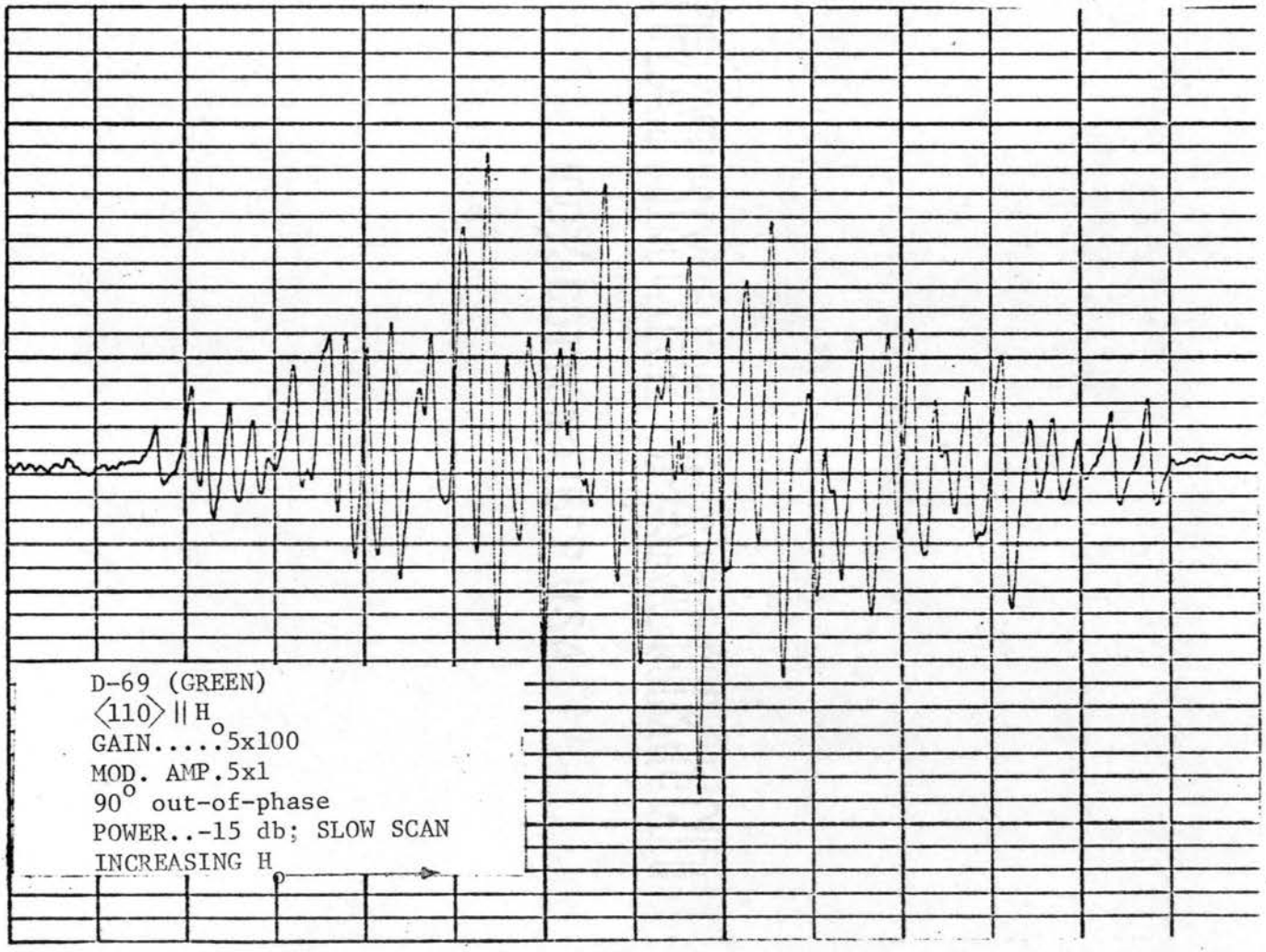

Figure 30. Electron spin resonance of complex center in D-69 (GREEN).

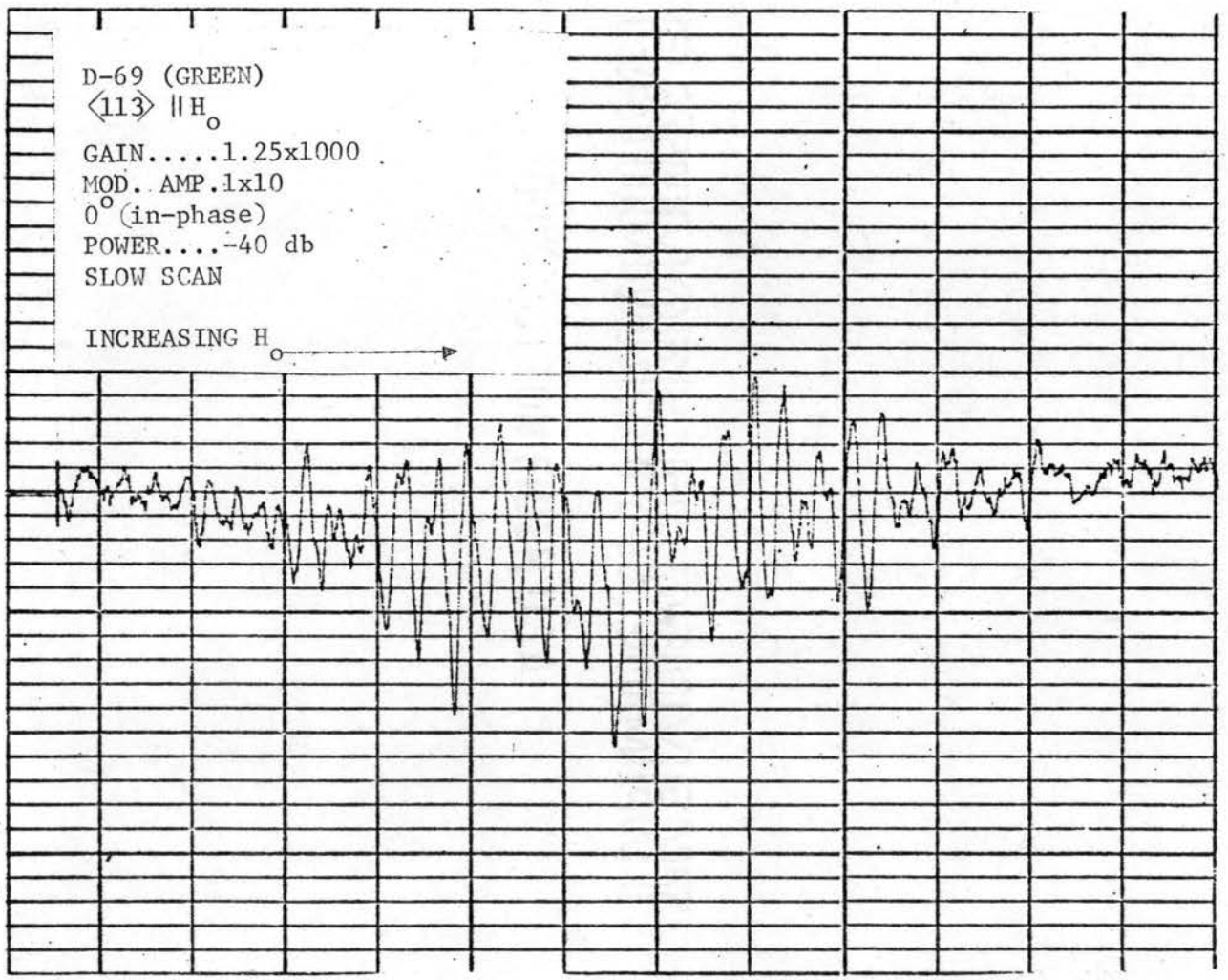

Figure 31. Electron spin resonance of complex center in D-69 (GREEN).

VITA

Sam E. Giuoco

Candidate for the Degree of

Master of Science

Thesis: CORRELATION OF COLOR AND ELECTRON SPIN RESONANCE IN DIAMOND

Major Field: Physics

Biographical:

Personal Data: Born in Pharr, Texas, September 26, 1940, the son of Frank and Odell Giuoco.

Education: Attended grade school in Pharr, Texas; graduated from Pharr-San Juan-Alamo High School in 1959; attended San Antonio College in San Antonio, Texas, 1964; received the Bachelor of Science degree from Pan American College, with majors in Physics and Mathmatics, in January, 1968; completed requirements for the Master of Science Degree in May, 1969.

Experience: Employed as a laboratory assistant in the physics department of Pan American College, Edinburg, Texas (1964-1968); graduate teaching assistant in the physics department of Oklahoma State University (1968-1969).

Organizations: Member of Sigma Pi Sigma, Society of Physics Students, and Mathematical Association of America.